Explicit Forecasts of Winter Precipitation Using an Improved Bulk Microphysics Scheme. Part I: Description and Sensitivity Analysis

GREGORY THOMPSON, ROY M. RASMUSSEN, AND KEVIN MANNING

National Center for Atmospheric Research, Boulder, Colorado

(Manuscript received 26 December 2002, in final form 19 September 2003)

ABSTRACT

This study evaluates the sensitivity of winter precipitation to numerous aspects of a bulk, mixed-phase microphysical parameterization found in three widely used mesoscale models [the fifth-generation Pennsylvania State University–National Center for Atmospheric Research Mesoscale Model (MM5), the Rapid Update Cycle (RUC), and the Weather Research and Forecast (WRF) model]. Sensitivities of the microphysics to primary ice initiation, autoconversion, cloud condensation nuclei (CCN) spectra, treatment of graupel, and parameters controlling the snow and rain size distributions are tested. The sensitivity tests are performed by simulating various cloud depths (with different cloud-top temperatures) using flow over an idealized two-dimensional mountain. The height and width of the two-dimensional barrier are designed to reproduce an updraft pattern with extent and magnitude consistent with documented freezing-drizzle cases. By increasing the moisture profile to saturation at low temperatures, a deep, precipitating snow cloud is also simulated. Upon testing the primary sensitivities of the microphysics scheme in two dimensions as reported in the present study, the MM5 with the modified scheme will be tested in multiple case studies and the results will be compared to observations in a forthcoming companion paper, Part II.

The key results of this study are 1) the choice of ice initiation schemes is relatively unimportant for deep precipitating snow clouds but more important for shallow warm clouds having cloud-top temperature greater than −13°C, 2) the assumed snow size distribution and associated snow diffusional growth along with the assumed graupel size distribution and method of transforming rimed snow into graupel have major impacts on the mass of cloud water and formation of freezing drizzle, and 3) a proper simulation of drizzle using a single-moment scheme and exponential size distribution requires an increase in the rain intercept parameter, thereby reducing rain terminal velocities to values more characteristic of drizzle.

1. Introduction

Numerical weather prediction of winter precipitation has been consistently improving over the past two decades, though there are still occasional ''bust'' forecasts. Advancing technology allows increasingly sophisticated physics to be incorporated into numerical models of increasing resolution. The representation of cloud microstructure and resulting hydrometeor evolution is no exception, using either explicit bin-resolving cloud models (Young 1974; Hall 1980; Kogan 1991; Feingold et al. 1988, 1994; Geresdi 1998; Rasmussen et al. 2002) or bulk microphysical parameterizations (Lin et al. 1983; Rutledge and Hobbs 1983, 1984; Cotton et al. 1986; Ferrier 1994; Kong and Yau 1997; Reisner et al. 1998). Bin models prognose multiple variables for specific intervals of each hydrometeor species size spectrum and are therefore extremely expensive in terms of computer time and memory. For this reason, bin models are not yet viable for real-time NWP efforts, though continued technological advances are likely to change this in the future. Alternatively, models designed for real-time applications utilize bulk microphysical parameterizations that reduce the number of prognostic variables by assuming hydrometeor size spectra follow a prescribed exponential (Kessler 1969) or gamma distribution (Verlinde et al. 1990; Walko et al. 1995).

Development and testing of bulk microphysical schemes tend to conform to one or two of the following scenarios: 1) clouds produced by deep convection (Lin et al. 1983; Murakami 1990; Ferrier 1994; Walko et al. 1995; Meyers et al. 1997; Swann 1998), 2) clouds associated with cold and/or warm fronts (Rutledge and Hobbs 1983, 1984; Reisner et al. 1998; Tremblay et al. 2001), or 3) clouds produced by orographic lift (Cotton et al. 1986; Meyers and Cotton 1992; Meyers et al. 1992). In the first two scenarios above, there tends to be tropospheric deep and strong ascent (vertical velocities ~1–10 m s^{-1}), while the third scenario generally involves weaker lift by comparison (~0.3–1 m s^{-1}) but equally cold cloud tops (temperature <-40°C).

In general, relatively deep and cold cloud system sim-

Corresponding author address: Gregory Thompson, NCAR-RAP, P.O. Box 3000, Boulder, CO 80301-3000.
E-mail: gthompsn@ucar.edu

ulations have abundant ice and snow that may mask subtle dependencies of a microphysical parameterization to produce supercooled liquid water. In many ways, simulations of deep precipitating storm systems are ''forgiving'' of subtle sensitivities within a microphysics scheme since there is abundant lift and abundant precipitation. Where quantitative precipitation forecasts are concerned, these sensitivities are relatively unimportant. However, in the aircraft operations arena, for example, they are critical to predicting whether airframe icing occurs or not. If the simulated cloud is composed primarily of snow, then liquid water is depleted, in which case little or no aircraft icing is predicted to occur. In contrast, the absence of ice and snow typically leads to development of supercooled cloud liquid water, or worse, supercooled drizzle (Cober et al. 2001).

The ultimate goal of the research reported in this paper is to improve explicit, real-time forecasts of supercooled liquid water and hence improve forecasts of aircraft icing. To accomplish this goal, the bulk, mixed-phase microphysical parameterization described in Reisner et al. (1998, hereafter RRB) is rigorously tested and improved. Each modification to RRB is discussed in section 2. Sensitivity tests are performed similar to Rasmussen et al. (2002, hereafter RG) using idealized flow over a two-dimensional barrier, and the scheme is tuned to results of the bin model of the aforementioned study. However, to ensure the model is not overly tuned to produce liquid instead of ice, we also perform tests of deeper and colder cloud systems. The implementation details are found in section 3, while section 4 contains the results of numerous 2D sensitivity experiments. Section 5 provides conclusions and a discussion of related, future topics. Most of the bulk microphysical studies mentioned earlier used a single case study for their test. In a forthcoming companion paper, Part II, the final scheme is tested on multiple case studies involving cloud systems of various temperatures/depths from a number of field projects from different geographical regions of the United States.

2. Description of the bulk microphysics parameterization

The bulk microphysical parameterization used in this study is an upgraded version of the scheme presented in RRB. Although it is available in three widely used mesoscale models, its development and testing are primarily performed using the fifth-generation Pennsylvania State University–National Center for Atmospheric Research (PSU–NCAR) Mesoscale Model (MM5), with results propagated to the Rapid Update Cycle (RUC; cf. Benjamin et al. 2004) and Weather Research and Forecasting (WRF) models. In RRB, this scheme is described as ''option 4'' (referred to as ''Reisner2'' by MM5 users) and is currently the most complex microphysics option available in the MM5 code distributed to the user community. Option 4 is a bulk, mixed-phase microphysics scheme with prognostic variables for the mixing ratios of cloud water (q_c), rain (q_r), cloud ice (q_i), snow (q_s), and graupel (q_g), plus the number concentration of ice (N_i). To date, the version described in RRB as ''option 5,'' which additionally prognoses number concentrations of graupel and snow, is not widely available and is therefore not considered in this study. Furthermore, the additional computational cost of option 5 inhibits its use for real-time applications as desired for the RUC and WRF models. Improvements and modifications to RRB are discussed below, while a number of additional, relatively minor alterations and corrections are included in the appendix.

a. Initiation of cloud ice

The nucleation of cloud ice due to deposition and condensation freezing previously used a relationship described in Fletcher (1962) as follows:

$$N_{i,\text{Fletcher}} = 10^{-5} \exp[0.6(T_0 - T)], \quad (1)$$

where $T_o = 273.15$ K, T is the ambient temperature (K), and N_i is the number of ice crystals initiated (L^{-1}). As mentioned in RRB, this relationship produces erroneously high concentrations of ice particles at very low temperatures; thus, ice number concentration was thresholded at the value attained when $T = 246$ K. For the current study, the Fletcher curve is replaced by a similar relationship determined by Cooper (1986) based on direct ice crystal measurements and given by

$$N_{i,\text{Cooper}} = 0.005 \exp[0.304(T_0 - T)]. \quad (2)$$

Similar to the low-temperature cutoff mentioned above, the number of ice crystals initiated is prevented from exceeding the value attained when $T = 233$ K. Both relationships are tested in sensitivity experiments discussed later as well as an alternate methodology for ice initiation described in Meyers et al. (1992) and given by

$$N_{i,\text{Meyers}} = \exp(-0.639 + 0.1296 S_i), \quad (3)$$

where S_i is the supersaturation (percent) with respect to ice. A depiction of these three relationships is found in Fig. 1 and reveals an order of magnitude or greater difference among them for temperatures between $-5°$ and $-15°$C but nearly the same concentration of ice near $-25°$C. The schemes again differ by nearly an order of magnitude below approximately $-50°$C. Note in Fig. 1 that the line shown for $N_{i,\text{Meyers}}$ assumes maximum possible S_i (i.e., water saturation).

A related, fundamental shift in ice initiation pertains to the necessary conditions to nucleate ice. Previously, ice was allowed to initiate by Eq. (1) as soon as ice saturation was attained for all temperatures less than 0°C. In the current scheme, ice does not form by Eq. (2) until the air is saturated with respect to water and $T < -5°$C or until the water vapor mixing ratio exceeds 5% supersaturation with respect to ice. However, as in

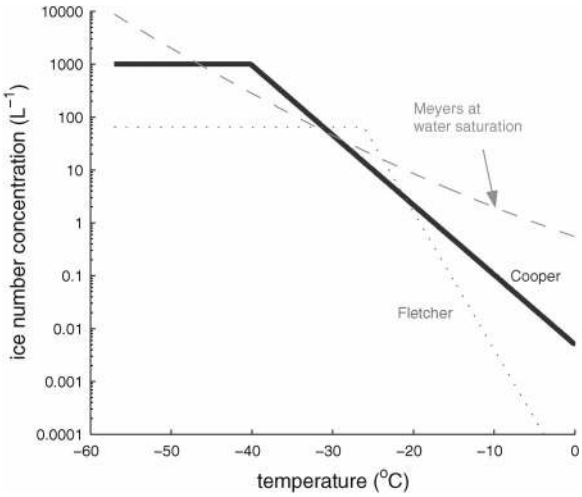

FIG. 1. Ice nucleation by deposition and condensation freezing as a function of temperature given by Fletcher (1962), Cooper (1986), and Meyers et al. (1992) at water saturation. Note that the variability exceeds an order of magnitude at relatively high temperatures.

RRB, ice continues to be formed by freezing of cloud droplets ($T < -5$°C) and by a secondary ice-nucleation method, commonly referred to as rime-splinter ice production, based on work by Hallet and Mossop (1974).

b. Autoconversion

The collision and coalescence of cloud droplets to form raindrops is parameterized by autoconverting between the mixing ratios of the two hydrometeor species, q_c and q_r, following Kessler (1969) and given by

$$\frac{dq_r}{dt} = aH(q_c - q_{\text{co}}), \tag{4}$$

where $a = 1 \times 10^{-3}$ s^{-1} is a time constant, H is a Heaviside function, and $q_{\text{co}} = 0.35 \times 10^{-3}$ is a threshold value. Previously, the threshold used in RRB was 0.5×10^{-3} but is reduced based on results by RG. Besides testing the old and revised thresholds, an additional sensitivity test is performed with $q_{\text{co}} = 0.1 \times 10^{-3}$.

As an alternative to the Kessler autoconversion scheme, the methodology described by Berry (1968) is also evaluated using the relationship

$$\frac{dQ_r}{dt} = \frac{Q_c^2}{2 + \left(\frac{0.0266}{D_b}\right)\left(\frac{N_b}{Q_c}\right)}, \tag{5}$$

where Q_r is the rain water content (g m^{-3}), $D_b = 0.3$ is the dispersion factor, N_b is cloud droplet concentration (cm^{-3}), and Q_c is the cloud water content (g m^{-3}).

In another, alternative autoconversion scheme, Walko et al. (1995) adapted a Berry and Reinhardt (1974) parameterization using the relationship[1]

$$\frac{dq_r}{dt} = \frac{2.7 \times 10^{-2} q_c \left[\frac{1}{16} \times 10^{20} D_{\text{mean}}^4 (1 + \upsilon)^{-0.5} - 0.4\right]}{\frac{3.7}{\rho_a q_c}[0.5 \times 10^6 D_{\text{mean}}(1 + \upsilon)^{-1/6} - 7.5]^{-1}}, \tag{6}$$

where υ represents a gamma distribution shape parameter, ρ_a and ρ_w are the density of air and water (kg m^{-3}), respectively, and D_{mean} is the mean diameter (m) of cloud droplets computed from cloud water mixing ratio (q_c) and concentration (N_c) using

$$D_{\text{mean}} = \left(\frac{6\rho_a q_c}{\pi \rho_w N_c}\right)^{1/3}. \tag{7}$$

In our application of Eq. (6), υ is set to 3, and both the numerator and denominator must be positive. Substituting various droplet concentrations of 50, 100, 200, and 500 cm^{-3} into Eqs. (6) and (7), we compute minimum cloud water mixing ratios of 0.171, 0.343, 0.686, and 1.71 g kg^{-1}, respectively, before cloud water converts to rain. Hence, Eq. (6) simplifies to a form similar to the Kessler autoconversion scheme with constant N_c, but the rates of rain conversion tend to be lower using Eq. (6) compared to Eq. (4). Nonetheless, this alteration is desireable because of its physical basis and for other/future modeling studies where N_c could be prognosed.

c. Treatment of graupel

In RRB, the size distribution of graupel assumed an exponential form [$N(D) = N_{o,g}\, e^{-\lambda_g D}$] with a constant intercept parameter ($N_{o,g} = 4 \times 10^6$ m^{-4}), whereas, in the current study, the distribution is altered in two ways. First, the distribution assumes the following generalized gamma form

$$N(D) = N_{o,g} D^{(\upsilon-1)} e^{-\lambda_g D}, \tag{8}$$

where

$$\lambda_g = 1.32\left(\frac{\pi \rho_g N_{o,g}}{\rho q_g}\right)^{0.2} \quad \text{and} \tag{9}$$

$$N_{o,g} = 2.38\left(\frac{\pi \rho_g}{\rho q_g}\right)^{0.92} \tag{10}$$

replace the slope and intercept parameters of the exponential distribution, $\upsilon = 2$, and $\rho_g = 400$ kg m^{-3} is the density of graupel. Second, $N_{o,g}$ depends on q_g similar to the RRB approach for determining $N_{o,s}$ as a function of q_s. Whereas the RRB study used observations

[1] This equation corrects three errors found in Walko et al. [1995, Eqs. (74)–(76)] and one error found in Berry and Reinhardt [1974, Eq. (16)].

by Sekhon and Srivastava (1970) to derive $N_{o,s} = f(q_s)$, we derive Eq. (10) using observations from Brown and Swann (1997). Note that because $N_{o,g} \rightarrow \infty$ as $q_g \rightarrow 0$, we limit the magnitude of $N_{o,g}$ such that it cannot exceed a fixed maximum value (5×10^7 m^{-4}) while also imposing a lower limit of 1×10^4 m^{-4}.

Besides the modification to the shape of the graupel distribution, the conversion of rimed snow into graupel is altered from the RRB study. In RRB, Eq. (A.43) contains the model time step, Δt, potentially requiring tuning when the time step is adjusted. In the current study, we follow the treatment found in Murakami (1990) and evaluate the larger of two terms: depositional growth (PSDEP) and riming growth (PSACW) of snow, computed as in Rutledge and Hobbs (1983) using

$$\text{PSDEP} = \frac{4(S_i - 1)N_{o,s}}{A + B} \times \left[\frac{0.65}{\lambda_s^2} + 0.44 S_c^{1/3} \left(\frac{a_s \rho}{\mu} \right)^{1/2} \frac{\Gamma\left(\frac{b_s}{2} + \frac{5}{2} \right)}{\lambda_s^{b_s/2+5/2}} \right], \quad (11)$$

and

$$\text{PSACW} = \frac{\rho \pi a_s q_c E_{sc} N_{o,s}}{4} \frac{\Gamma(b_s + 3)}{\lambda_s^{b_s+3}}, \quad (12)$$

respectively, where A and B are thermodynamic terms given in Pruppacher and Klett (1978), $S_c = 0.6$ is the Schmidt number, $a_s = 11.72$ m$^{(1-b_s)}$ s^{-1} and $b_s = 0.41$ are constants in the snow fall speed relation, E_{sc} is the collection efficiency between snow and cloud water, λ_s is the slope of the snow size distribution (m^{-1}) and μ is the dynamic viscosity of air (kg m^{-1} s^{-1}). If riming growth exceeds depositional growth, then graupel increases at the rate given by PSACW, otherwise snow increases at this rate. To illustrate the relative contributions by these two terms, Fig. 2 presents PSDEP contours as a function of snow mixing ratio and temperature (Fig. 2a), PSACW contours as a function of snow and cloud water mixing ratios (Fig. 2b), and the ratio of the two at $T = -10$°C (Fig. 2c). In general, riming growth does not exceed depositional growth until cloud liquid water exceeds 0.1 g kg^{-1}. Rutledge and Hobbs (1984) required a threshold snow mixing ratio of 0.1 g kg^{-1} and a cloud water mixing ratio threshold of 0.5 g kg^{-1} before producing graupel. These thresholds approximately correspond to PSDEP/PSACW = 0.2 curve shown in Fig. 2c, implying that riming growth must exceed depositional growth by a factor of 5 before rimed snow transitions to the graupel category.

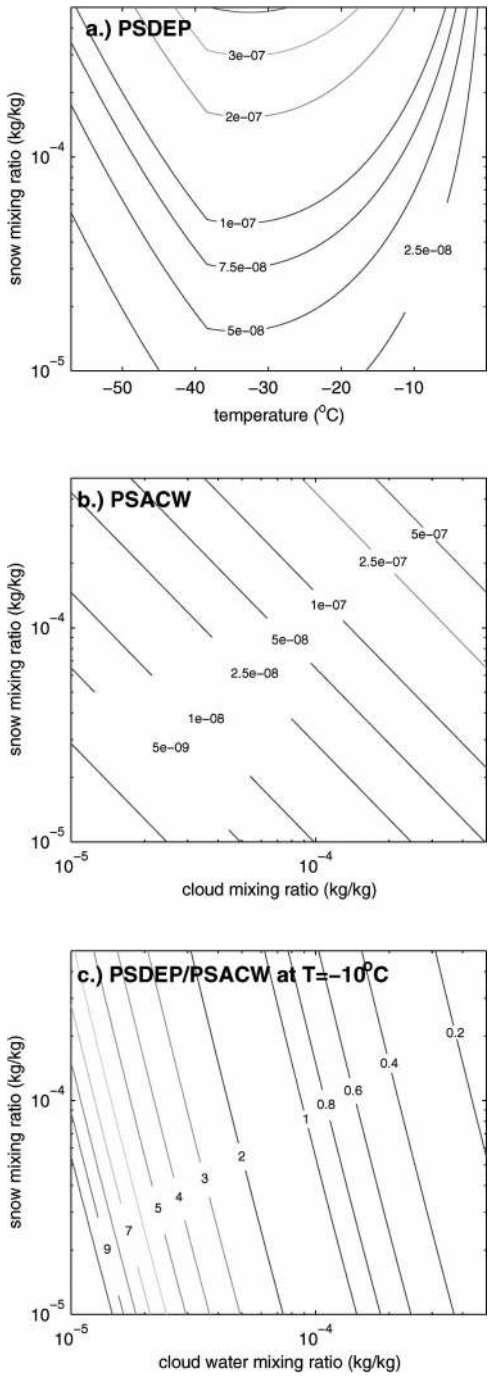

FIG. 2. Contours of (a) PSDEP (kg kg^{-1} s^{-1}) as a function of mixing ratio and temperature, (b) PSACW (kg kg^{-1} s^{-1}) as a function of snow and cloud water mixing ratio, and (c) the ratio of PSDEP/PSACW at $T = -10$°C. Note in (c) that depositional growth generally exceeds riming growth until cloud liquid water increases to appreciable amounts typically associated with drizzle or rain formation.

d. Intercept parameter of the snow size distribution

RRB determined that a fixed snow intercept parameter led to the depletion of too much cloud water, therefore motivating the mass-dependent $N_{o,s}$ relationship used previously in MM5. Similarly, Swann (1998) utilized snow and graupel intercept parameters that depended on mixing ratio in a single-moment microphysics

scheme; however, he speculated that a temperature or height dependence may improve the scheme to match results from a double-moment scheme. By analyzing 37 particle-size spectra from aircraft flights through frontal clouds at virtually all temperatures aloft, Houze et al. (1979) found that mean particle diameter increased with increasing temperature, and, more importantly, N_o and λ decreased with increasing temperature as a result of growth by aggregation. Thus, we decided to implement an explicit temperature-dependent $N_{o,s}$ into the scheme using the curve for total precipitation water content $0.03 \leq M < 0.3$ in Fig. 7 of Houze et al. (1979), resulting in the following relationship:

$$N_{o,s} = \min\{2 \times 10^8, 2 \times 10^6 \times \exp[-0.12 \min(-0.001, T - T_o)]\}, \quad (13)$$

where $T_o = 273.15$ K, and T is the ambient temperature (K). Considering that this version of the microphysics code lacks a snow aggregate species, perhaps a temperature-dependent $N_{o,s}$ is the simplest way to parameterize this effect. Alternatively, the addition of an aggregate species and associated prognostic equations could be developed.

The largest impact of the new relationship for $N_{o,s}$ pertains to depositional growth of snow [PSDEP; Eq. (11)], which is illustrated in Fig. 3. In Fig. 3a, the vertical profile of snow mixing ratio varies from 0.002 to 0.2 g kg^{-1}, corresponding to a hypothetical, shallow, mixed-phase cloud. Note that the maximum $N_{o,s}$ exceeds the old value by an order of magnitude at low temperatures; thus, the depositional growth is larger at temperatures < -20°C using the new method. However, in relatively warm air ($T > -20$°C), the intercept parameter is less using the new method, and therefore depositional growth is reduced. On the other hand, when the vertical profile of snow mixing ratio more closely mimics a deep snow cloud with q_s ranging from 0.05 to 0.5 g kg^{-1} (corresponding to Fig. 3b), then PSDEP is always larger using the temperature-dependent relationship over the mass-dependent $N_{o,s}$.

Whereas the maximum depositional growth of a single ice crystal generally peaks around $T = -14$°C (see, e.g., Wallace and Hobbs 1977 or Young 1993), Figs. 2a and 3 represent the aggregate effect of depositional growth on an entire snow size distribution. The very broad minimum centered at -35°C in Fig. 2a and maximum at approximately -20°C in Fig. 3 are a result of the increase in $N_{o,s}$ with decreasing temperature [Eq. (13)]. In other words, a population of large numbers of small snow crystals at $T = -30$°C grows nearly as rapidly by deposition as a reduced number of larger crystals at higher temperatures.

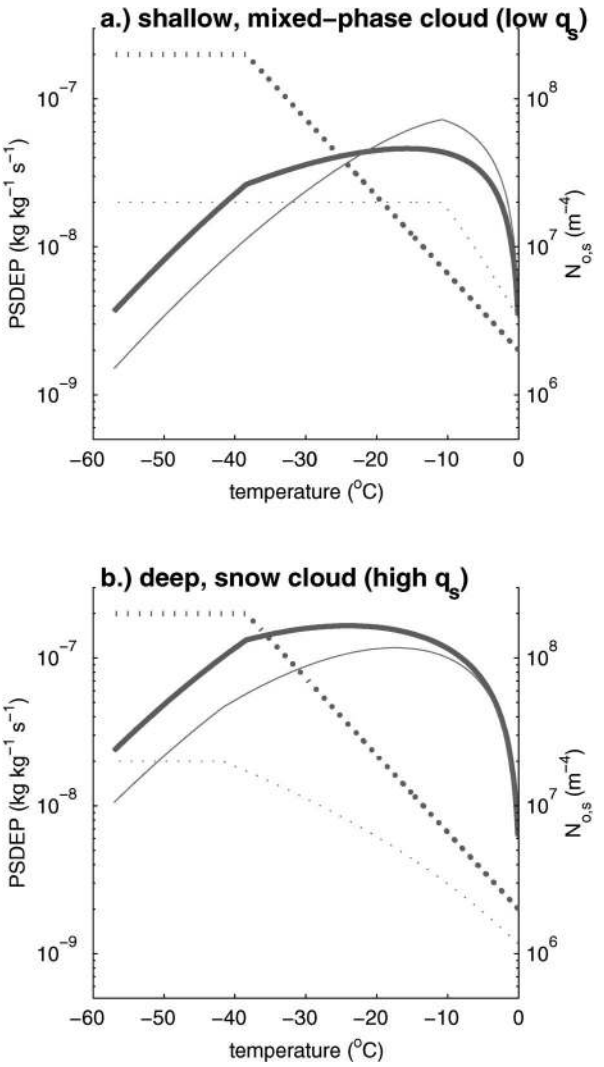

FIG. 3. PSDEP (solid) and snow size distribution intercept parameter ($N_{o,s}$ dotted) vs temperature using the new temperature-dependent $N_{o,s}$ (thick lines/dots) given by Eq. (13) and original mass-dependent $N_{o,s}$ (thin lines/dots) relationship given by Reisner et al. (1998). In (a), the snow mixing ratio varies between 0.002 and 0.2 g kg^{-1} as in a typical, shallow, mixed-phase cloud, and depositional growth is lower at relatively high temperatures using the new scheme rather than the old scheme. In (b), the snow mixing ratio varies between 0.05 and 0.5 g kg^{-1} as in a typical, deep, precipitating snow cloud, and depositional growth is always larger using the new scheme rather than the old.

e. Intercept parameter of the rain size distribution

Unlike the intercept parameter for snow, previous studies do not support a temperature-dependent rain size distribution. Instead, it is quite reasonable to assume that water drops undergo a gradual transition from cloud droplet sizes (diameter less than approximately 50 μm) through drizzle drops (diameter approximately 50–500 μm) on their way to becoming raindrops. However, nearly all single-moment bulk microphysics schemes simply make an abrupt transition from cloud water to rain with the associated Marshall–Palmer size distribution and intercept parameter of 8×10^6 m^{-4}. Thus liquid drops undergo a transition from nonsettling (most bulk microphysics schemes do not sediment cloud droplets) to typ-

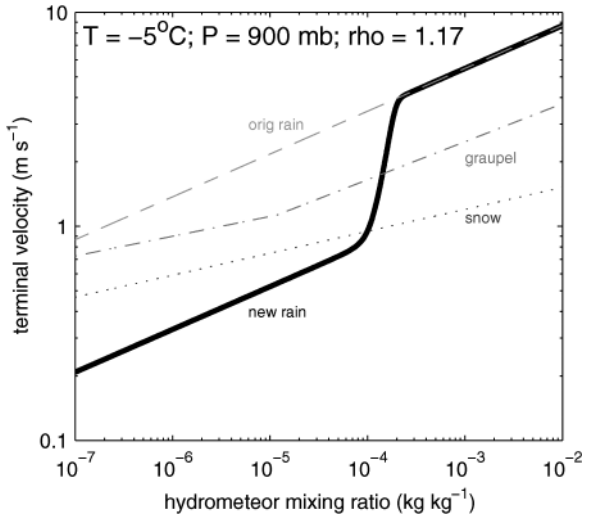

FIG. 4. Mass-weighted terminal velocity vs mixing ratio for hydrometeor species: snow, graupel, and rain at 900 hPa and $T = -5°C$. The dashed line labeled ''orig. rain'' indicates the terminal velocity for rain using a constant value of $N_{o,r} = 8 \times 10^6$ m^{-4}, while the solid, thick line labeled ''new rain'' uses the new mass-dependent relationship in Eq. (14) (tested in sensitivity test RONV).

ical rain terminal velocities of 1–4 m s^{-1} instantaneously. This leaves little time for water drops to interact as drizzle drops with other microphysical species such as snow, graupel, and cloud water. Instead, raindrops race to hit the earth as precipitation and rarely remain suspended within gentle stratiform updrafts. With these considerations in mind, we alter the rain size distribution via the intercept parameter to replicate a drizzle transition whereby the size distribution of rain consists primarily of drizzle-size drops for very low rain mixing ratios. On the other hand, when rain mixing ratio increases, the intercept parameter decreases, thus broadening the rain distribution and replicating the original formulation. The following function encapsulates the transition of the intercept parameter from drizzle to rain:

$$N_{o,r} = \left(\frac{N_{1,r} - N_{2,r}}{2}\right) \tanh\left[\frac{4(q_{\text{ro}} - q_r)}{q_{\text{ro}}}\right] + \frac{N_{1,r} + N_{2,r}}{2}, \quad (14)$$

where $N_{1,r} = 1 \times 10^{10}$ m^{-4} is an upper-intercept limit, $N_{2,r} = 8 \times 10^6$ m^{-4} is a lower-intercept limit, and $q_{\text{ro}} = 1 \times 10^{-4}$ is essentially the transition value between the two limits. The terminal velocity that results when $N_{o,r}$ spans this range is shown in Fig. 4 (labeled as ''new rain'') along with the curve for the original terminal velocity using the previously fixed value of $N_{o,r}$ and curves for terminal velocities of snow and graupel. The graph shows the primary result of a varying $N_{o,r}$ is that small q_r (theoretically more common of drizzle rather than rain) produce a terminal velocity between 0.2 and 2 m s^{-1}, whereas large rain mixing ratios produce terminal velocities between 2 and 8 m s^{-1}. According to Young (1993), the former velocities correspond to drops with diameters between 50 and 200 μm, while the latter velocities correspond to drops with diameters between 200 μm and 1 mm. Results of sensitivity tests for this and all other alterations are presented in section 4.

3. Approach

As discussed in the introduction, a primary goal of this study is to reproduce the results found by RG using a bulk microphysics parameterization in place of the computationally demanding detailed model. To accomplish this, a two-dimensional version of the PSU–NCAR Mesoscale Model is configured nearly identically to the RG study. The MM5 domain is 120 points wide, spaced 10 km apart, by 39 σ_p vertical levels, with effective spacing of 40 m at the surface stretching to a constant 900 m from 5 km to the model top at 100 hPa. Flow of 15 m s^{-1} impinges upon a bell-shaped mountain 1 km high with a 100-km half-width. The initial temperature and moisture profiles (thick solid lines shown in Fig. 5a) are modified slightly from the RG study in order to vary the moisture in a realistic manner to create clouds of varying depths and temperatures. The temperature and moisture profiles below the barrier height are identical in the two studies, but the inversion between 1 and 3 km is slightly warmer (1°–2°C) and drier in this study compared to the inversion found in RG (thick, dashed lines in Fig. 5a represent the temperature and moisture profiles used in RG). Furthermore, the temperature profile above the inversion differs significantly from the RG sounding but is not important for comparison purposes since the simulated cloud resides within and below the inversion. Previously, the lapse rate above the inversion was absolutely stable whereas the new lapse rate is conditionally unstable. This alteration allows for varying the depth of saturation to simulate a deep precipitating snow cloud as well as the relatively warm cloud top as in the RG study. Alternatively, we could have used the RG sounding while increasing the moisture to saturation, but this would have created an unrealistic profile for a deep precipitating snow cloud. As expected, there are minor differences between the simulation using the new sounding and a simulation using the RG sounding. The new sounding results in a slightly warmer and shallower cloud: cloud-top temperature (CTT) reaches −13°C using the modified sounding versus CTT = −14°C using the original RG sounding.

Table 1 presents the simulation experiments performed using the new sounding discussed above. As shown, sensitivities of the microphysics to primary ice initiation, autoconversion, and continental and maritime cloud condensation nuclei (CCN) spectra, treatment of graupel, and parameters controlling the snow and rain size distributions are tested. The code used in the simulation referred to throughout as ''CONTROL'' includes Cooper ice initiation given by Eq. (2), whereas the

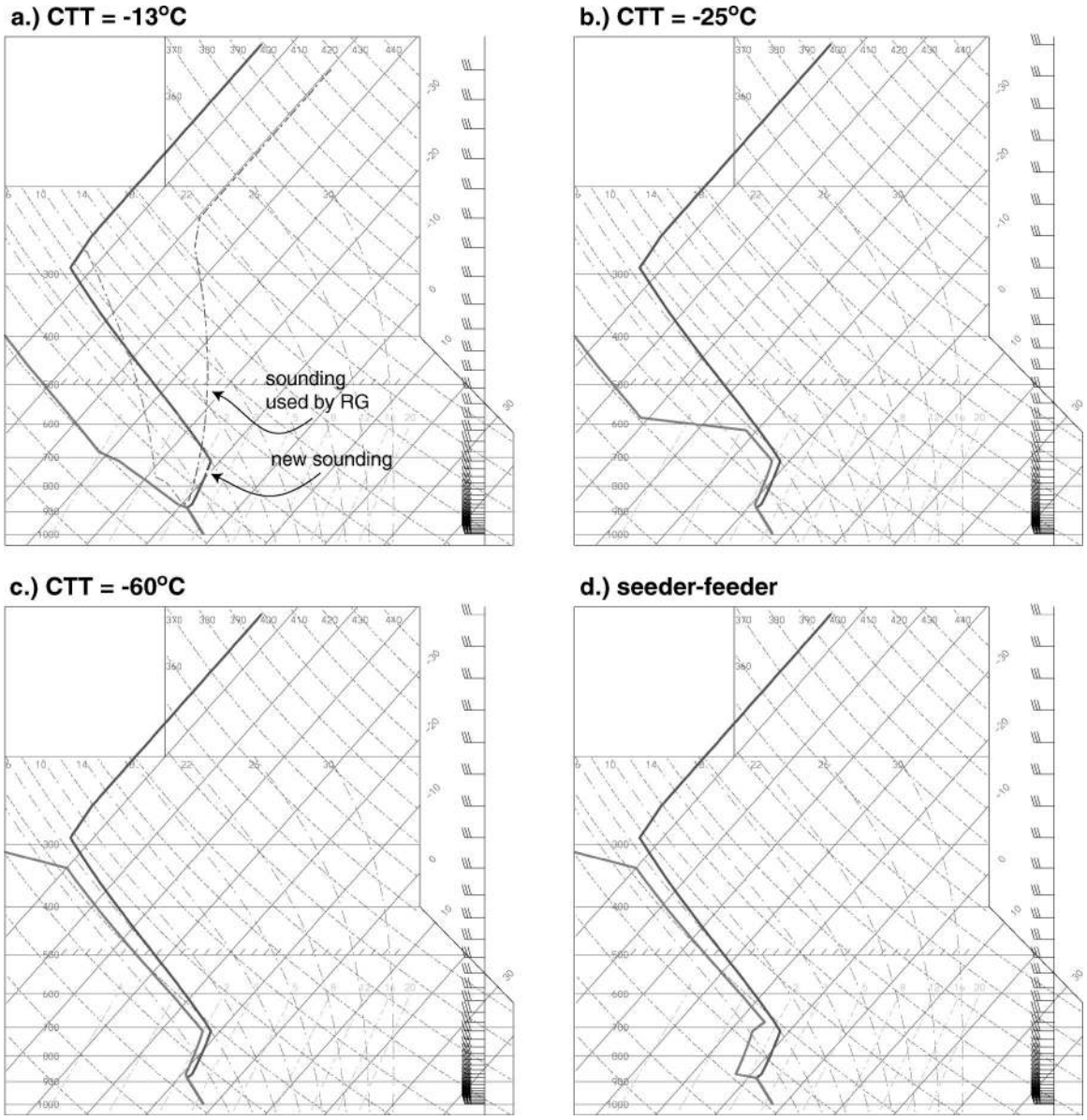

FIG. 5. Initial soundings used in MM5 2D idealized-flow sensitivity tests. The soundings produce clouds with: (a) CTT = −13°C, (b) CTT = −25°C, (c) CTT = −60°C, and (d) seeder–feeder cloud system. Wind barbs are plotted at every model σ level, with a full barb representing 5 m s^{-1}.

Fletcher and Meyers ice initiation schemes are tested in sensitivity experiments referred to as ''Fletcher'' and ''Meyers,'' respectively. CONTROL also uses the Kessler autoconversion scheme of Eq. (4) with cloud water mixing ratio threshold set to 0.35×10^{-3}, whereas the threshold is lowered in an experiment called ''Kessler1'' and then raised in experiment ''Kessler5.'' To test further the sensitivity to autoconversion, the Berry scheme of Eq. (5) is used in an experiment called ''Berry'' and the Berry and Reinhardt scheme of Eq. (6) is run as experiment ''BandR.'' Autoconversion and CCN spectra are linked via the relationship between cloud water mixing ratio and concentration [Eq. (7)]. Therefore, in association with the BandR simulation, the number concentration of cloud droplets (set to 100 cm^{-3} in CONTROL) is decreased to 50 cm^{-3} in the ''Maritime'' experiment, then increased to 200 cm^{-3} in ''Continental1'' and increased again to 500 cm^{-3} in ''Continental2.'' CONTROL uses the gamma size distribution for graupel, whereas an experiment called ''Graupel1'' uses the original exponential distribution and constant $N_{o,g}$ as in RRB. Furthermore, CONTROL requires riming growth of snow to exceed depositional growth before converting rimed snow into graupel, but Graupel1 uses the RRB formulation (containing the time step dependency) for this conversion process. Then, in a sensitivity experi-

TABLE 1. Summary of sensitivity experiments with alterations from CONTROL listed under brief description.

Experiment name	Brief description	CTT = −13°C	CTT = −25°C	CTT = −60°C	Seeder–feeder
CONTROL	Cooper ice initiation [Eq. (2)], Kessler autoconversion [Eq. (4); $q_{co} = 0.35 \times 10^{-3}$], $N_c = 100$ cm^{-3}, $N_{o,g} = f(q_g)$ [Eq. (10)], Murakami rimed snow-to-graupel conversion, $N_{o,s} = f(q_s)$, and $N_{o,r} = 8 \times 10^6$ m^{-4}.	×	×	×	×
Fletcher	Fletcher ice initiation [Eq. (1)].	×		×	
Meyers	Meyers ice initiation [Eq. (3)].	×		×	
Kessler1	Kessler autoconversion [Eq. (4); $q_{co} = 0.1 \times 10^{-3}$].	×			
Kessler5	Kessler autoconversion [Eq. (4); $q_{co} = 0.5 \times 10^{-3}$].	×			
Berry	Berry autoconversion [Eq. (5)].	×			
BandR	Berry and Reinhardt autoconversion [Eq. (6)].	×			
Maritime*	Maritime CCN spectra, $N_c = 50$ cm^{-3}.	×			
Continental1*	Continental CCN spectra, $N_c = 200$ cm^{-3}.	×			
Continental2*	Polluted continental CCN spectra, $N_c = 500$ cm^{-3}.	×			
Graupel1	Original exponential distribution, $N_{o,g} = 4 \times 10^6$ m^{-4}, and original Reisner rimed snow-to-graupel conversion.	×	×	×	×
Graupel2	Riming growth of snow must be 3 times larger than depositional growth before creating graupel.	×	×	×	×
Version2	Combine Fletcher, Kessler5, and Graupel1.	×	×		
SON	Constant $N_{o,s} = 2 \times 10^7$ m^{-4}.	×	×	×	×
SONV	$N_{o,s} = f(T)$ [Eq. (13)].	×	×	×	×
RON$^+$	Constant $N_{o,r} = 1 \times 10^{10}$ m^{-4}.	×			
RONV$^+$	$N_{o,r} = f(q_r)$ [Eq. (14)].	×			
Final	Combine BandR ($N_c = 100$ cm^{-3}), Graupel2, SONV, and RONV.	×	×	×	×

* Combines code used in BandR, and all ice physics are disabled.
+ Combines code used in SONV.

ment called ''Graupel2,'' the gamma distribution is reintroduced, but the riming growth must exceed depositional growth of snow by a factor of 3 before converting rimed snow to graupel. In RRB and CONTROL, the intercept parameter of snow is a function of snow mixing ratio, while a constant value is tested in ''SON,'' followed by a test using the temperature-dependent relationship of Eq. (13) in experiment ''SONV.'' Next, the intercept parameter for rain is constant in CONTROL but increased for experiment ''RON'' and altered to depend on rain mixing ratio by Eq. (14) in experiment ''RONV.'' Last, a sensitivity simulation combining modifications used in BandR (with $N_c = 100$ cm^{-3}), Graupel2, SONV, and RONV is performed in the experiment called ''Final.'' This combination represents the final bulk microphysics parameterization and is what we recommend for general use by modelers using this scheme, particularly MM5, RUC, and WRF real-time applications.

Besides CONTROL and the 17 sensitivity experiments that used the temperature and moisture profiles shown in Fig. 5a, additional simulations are performed with the same temperature profile but with moisture increased to saturation to various temperatures, thus producing cloud systems extending to the −25° and −60°C levels (Figs. 5b and 5c, respectively). Last, the moisture in the −60°C cloud-top temperature sounding is decreased to 3°C dewpoint below saturation between 1 and 3 km to simulate a seeder–feeder cloud system (Fig. 5d).

4. Sensitivity tests

a. CONTROL experiment

During the initial 30 min, a small cloud composed of water forms approximately two-thirds of the way up the barrier. This liquid cloud grows horizontally and vertically while a small amount of cloud ice is initiated near cloud top. Cloud water and cloud ice continue to increase during the first two hours of the simulation, with vertical growth to 2 km (approximately −13°C). Cloud ice rapidly grows by deposition to form snow that sediments and precipitates. Once snow forms, it accretes cloud water and rimes, thus increasing the mass of snow but also creating a comparable amount of graupel. The formation of graupel triggers ice multiplication (within the temperature range −3° to −8°C), which increases the background value of ice number concentration from 0.05 to 0.7 L^{-1}. These new ice crystals form directly within the liquid portion of the cloud and rapidly grow to snow sizes and accrete more cloud water. As snow and graupel continue to increase in mass, cloud water slowly depletes. Two hours into the CONTROL simulation, the cloud water peaks at 0.364 g kg^{-1}, just crossing the threshold quantity for autoconversion to the rain category (essentially becoming freezing drizzle). Thereafter, cloud water decreases as glaciation dominates, while snow and graupel precipitate in nearly equal proportions. A snapshot of the microphysical species: cloud water, cloud ice, snow, rain, and graupel at 3 h, along with a plot of precipitation type and amount at hours 3 and 4 are shown in

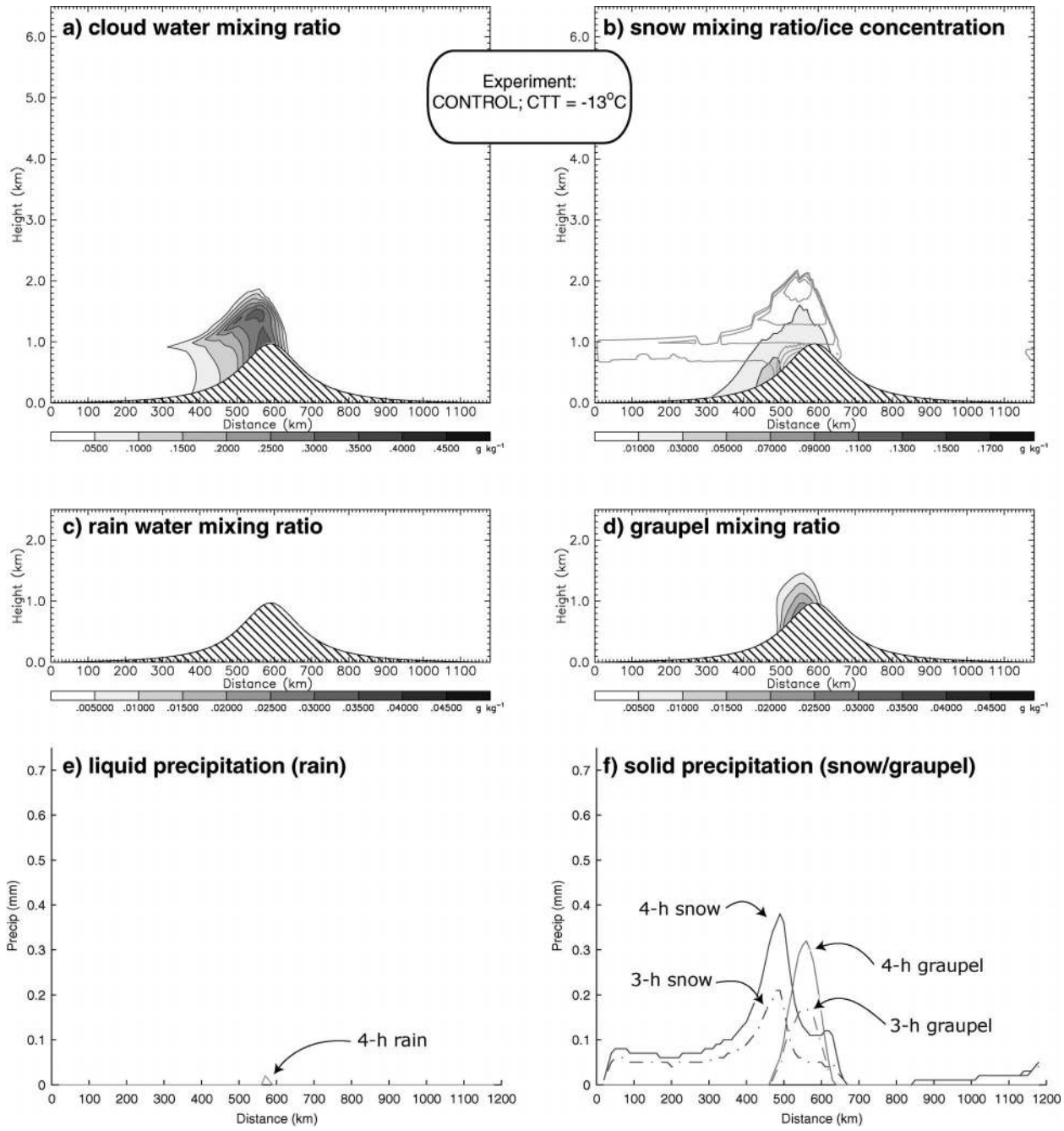

FIG. 6. Vertical cross sections from experiment CONTROL at 3 h using CTT = −13°C sounding (Fig. 5a): (a) cloud liquid water (g kg^{-1}), (b) snow mixing ratio (g kg^{-1}; shaded) with number concentration of ice (contours at 25, 50, 100, . . . m^{-3}), (c) rain mixing ratio (g kg^{-1}), and (d) graupel mixing ratio (g kg^{-1}). Also, precipitation accumulation since initial time vs distance at 3 h (dashed line) and 4 h (solid line) segregated by (e) rain (mm) and (f) snow and graupel (mm).

Fig. 6, while 3-h domain-maximum values of all hydrometeor species are listed in Table 2, along with 6-h simulation maxima shown in parentheses. The third value found in square brackets in each column is the rmse (L2 norm) computed as the square root of the sum (over all grid points) of squared differences between the bulk and bin models at 3 h.

b. Bin model

To compare directly between results of the bulk versus the bin models, we performed a new bin-model simulation using the CTT = −13°C sounding. While the bin model is capable of depleting ice nuclei, the bulk model is not; so, for proper comparison, we dis-

TABLE 2. Domain-maximum hydrometeor quantities at 3 h from 2D sensitivity simulations with CTT = −13°C, with 6-h maxima shown in parentheses and rmse shown in square brackets.

Sensitivity test	q_c (g kg^{-1})	q_i ($\times 10^{-3}$ g kg^{-1})	N_i (L^{-1})	q_r (g kg^{-1})	q_s (g kg^{-1})	q_g (g kg^{-1})
Bin model	0.290 (0.387)	0.03 (0.07)	0.3 (1.4)	0.035 (0.080)	0.040 (0.047)	0.014 (0.034)
CONTROL	0.339 (0.364) [2.05]	0.03 (0.06) [0.76]	0.4 (0.7) [0.42]	0.000 (0.002) [0.12]	0.045 (0.088) [0.23]	0.024 (0.025) [0.11]
Fletcher	0.343 (0.365) [2.07]	0.03 (0.03) [0.77]	0.4 (0.4) [0.41]	0.000 (0.002) [0.11]	0.044 (0.087) [0.23]	0.023 (0.025) [0.11]
Meyers	0.286 (0.349) [1.93]	0.19 (0.46) [2.18]	3.4 (4.3) [2.58]	0.000 (0.000) [0.12]	0.051 (0.088) [0.26]	0.024 (0.024) [0.10]
Kessler1	0.133 (0.174) [1.98]	0.02 (0.06) [0.77]	0.4 (0.7) [0.46]	0.007 (0.013) [0.09]	0.056 (0.079) [0.28]	0.007 (0.009) [0.02]
Kessler5	0.339 (0.383) [2.06]	0.03 (0.06) [0.76]	0.4 (0.7) [0.42]	0.000 (0.000) [0.12]	0.045 (0.088) [0.23]	0.024 (0.025) [0.11]
Berry	0.067 (0.090) [2.66]	0.02 (0.06) [0.77]	0.4 (0.7) [0.46]	0.010 (0.015) [0.10]	0.041 (0.066) [0.18]	0.013 (0.014) [0.04]
BandR	0.339 (0.383) [2.06]	0.03 (0.06) [0.76]	0.4 (0.7) [0.42]	0.000 (0.000) [0.12]	0.045 (0.088) [0.23]	0.024 (0.025) [0.11]
Graupel1	0.291 (0.353) [1.76]	0.02 (0.06) [0.78]	0.4 (0.7) [0.46]	0.000 (0.000) [0.12]	0.058 (0.078) [0.28]	0.012 (0.013) [0.05]
Graupel2	0.276 (0.336) [1.81]	0.02 (0.06) [0.78]	0.4 (0.7) [0.47]	0.000 (0.000) [0.12]	0.077 (0.084) [0.41]	0.000 (0.000) [0.04]
Version2	0.295 (0.356) [1.77]	0.21 (0.23) [1.13]	2.8 (3.1) [1.01]	0.000 (0.000) [0.12]	0.057 (0.077) [0.27]	0.012 (0.013) [0.05]
SON	0.339 (0.364) [2.05]	0.03 (0.06) [0.76]	0.4 (0.7) [0.42]	0.000 (0.002) [0.12]	0.048 (0.106) [0.23]	0.024 (0.025) [0.11]
SONV	0.381 (0.397) [2.36]	0.05 (0.08) [0.76]	0.8 (1.4) [0.43]	0.009 (0.011) [0.08]	0.006 (0.020) [0.20]	0.019 (0.033) [0.08]
RON	0.367 (0.386) [1.65]	0.05 (0.06) [0.78]	0.6 (1.5) [0.46]	0.065 (0.079) [0.18]	0.007 (0.028) [0.19]	0.014 (0.027) [0.06]
RONV	0.367 (0.386) [1.65]	0.05 (0.06) [0.77]	0.6 (1.5) [0.46]	0.064 (0.075) [0.18]	0.007 (0.028) [0.19]	0.014 (0.027) [0.06]
Final	0.386 (0.409) [1.60]	0.03 (0.06) [0.76]	0.5 (1.3) [0.44]	0.017 (0.017) [0.06]	0.064 (0.080) [0.21]	0.012 (0.017) [0.02]

abled ice nuclei depletion (as in RG simulation 10). In this manner, both the bin and bulk schemes initiate new ice crystals as the number concentration falls below the prescribed Cooper amount [Eq. (2) and Fig. 1]. As discussed in RG and graphically shown here in Fig. 7 and Table 2, this has important consequences to the resulting cloud water, rain, snow, and graupel amounts. The new bin-model simulation contains 4 times as much frozen hydrometeors (snow and graupel) and approximately one-half as much liquid compared to results shown in RG with ice nuclei depletion active. The sensitivity experiments described below illustrate the key modifications to the bulk scheme that bring the simulation into closer agreement with results of this new bin-model simulation.

c. Ice initiation: Meyers and Fletcher experiments

To illustrate the sensitivity of the microphysics parameterization to primary ice initiation, the model is modified to use the ice nucleation schemes of Meyers et al. (1992) and Fletcher (1962). The experiment called Meyers produces at least an order of magnitude more ice crystals throughout the cloud compared to CONTROL. The increase in ice number produces the anticipated result of less cloud water (~16%) and 14% more snow (Table 2). The Fletcher experiment, on the other hand, produces an order of magnitude reduction in ice number concentration at cloud top than CONTROL, resulting in marginally more cloud liquid water.

d. Autoconversion: Kessler1, Kessler5, Berry, and BandR experiments

The next series of tests involves the treatment of converting cloud water to the rain category by autoconversion using Kessler's methodology in Eq. (4), the Berry scheme in Eq. (5), and the Berry and Reinhardt scheme in Eq. (6). The Kessler autoconversion threshold is 0.35×10^{-3} in CONTROL, 0.1×10^{-3} in Kessler1, and 0.5×10^{-3} in Kessler5. Not unexpectedly, Kessler1 produces far less cloud water (maximum 0.133 g kg^{-1}), a lot more rain, and less graupel than CONTROL, as cloud water is readily converted to rain that precipitates quickly onto the ground. Kessler5 is hardly different from CONTROL since the updraft produced by this flow regime is only strong enough to produce a limited amount of cloud water that is depleted by snow and ice. The Berry experiment produces drastically smaller amounts of cloud water mixing ratio (maximum 0.067 g kg^{-1}), much more rain (accumulation ≈ 0.4 mm), and slightly less snow/graupel than CONTROL. The BandR experiment nearly matches CONTROL except for a slight increase in maximum cloud water and less rain because of its low autoconversion rate (when compared to the Kessler rate).

To see the true sensitivities of these autoconversion schemes, one needs to disable all the ice species/inter-

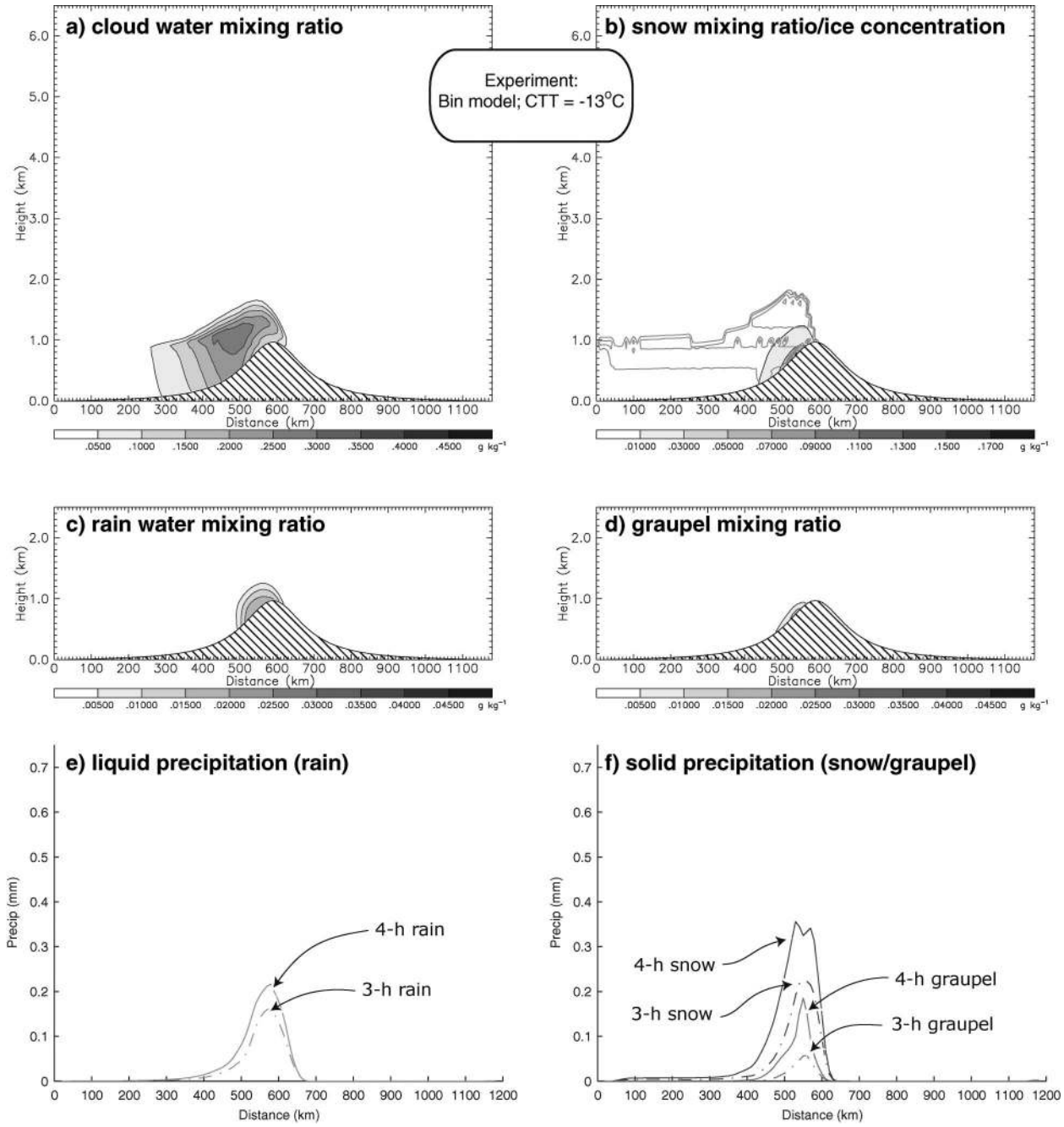

FIG. 7. Vertical cross sections at 3 h from the experiment using Rasmussen et al. (2002) bin microphysics model and CTT = −13°C sounding (Fig. 5a); otherwise same as Fig. 6.

actions and simulate the warm-rain process by itself. Results from this suite of tests with ice physics disabled produces the results shown in Fig. 8a. The same trend as mentioned above occurs with Kessler1 and Berry, showing very aggressive rain production initiating from the lowest cloud water amounts. CONTROL is next (not shown), followed by Kessler5, then BandR. It is also clear from this figure that BandR has the slowest rate of cloud water to rain conversion of all the experiments.

e. CCN spectra: Maritime, Continental1, and Continental2 experiments

The sensitivity of the microphysics to CCN spectra is addressed using three simulations with various cloud droplet concentrations (N_c, a proxy variable for CCN spectra). Since the Kessler (1969) autoconversion scheme does not include the effects of N_c, these tests are combined with the Berry and Reinhardt (1974) au-

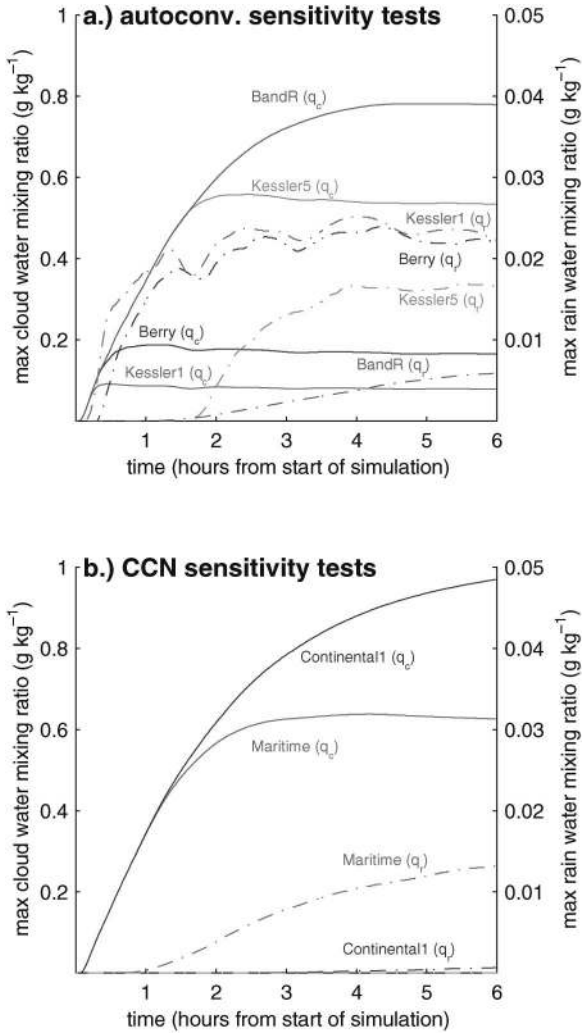

FIG. 8. Time series of cloud water (q_c—left abscissa; solid lines) and rain (q_r—right abscissa; dashed lines) mixing ratios (g kg^{-1}) from the set of (a) autoconversion and (b) CCN spectra experiments.

toconversion method discussed above in experiment BandR. Whereas CONTROL used $N_c = 100$ cm^{-3}, the Maritime experiment uses $N_c = 50$ cm^{-3}, Continental1 uses $N_c = 200$ cm^{-3}, and Continental2 uses $N_c = 500$ cm^{-3}. Like the previous test above, we disable all ice physics to prevent water depletion by ice and to compare against results of RG. As expected, the Maritime experiment produces the least cloud water and the most rain, while Continental2 produces the greatest cloud water mixing ratio and no rain (Fig. 8b). Direct comparisons to results by RG are found below (section 4i).

f. Treatment of graupel: Graupel1 and Graupel2 experiments

The treatment of graupel has major impacts on a mixed-phase simulation such as this one. Besides the assumed graupel size distribution, the treatment of snow riming and subsequent conversion to graupel is also important. In experiment Graupel1, the original exponential or Marshall–Palmer size distribution employed by RRB replaces Eqs. (8)–(10). Furthermore, the conversion of rimed snow to graupel is altered from the new methodology discussed in section 2 back to its original formulation as specified in RRB. Results of this test reveal a 14% reduction of cloud water, a 30% increase in snow, and 51% less graupel. Graupel is reduced primarily because its intercept parameter is constant and relatively low in Graupel1; therefore, depositional growth of graupel is reduced from that of CONTROL. Instead of growing graupel, deposition onto snow dominates, as evidenced by the accumulated precipitation plot (Fig. 9f) showing snow dominating between the third and fourth hour. None of the results discussed thus far matches those of RG, where the primary precipitation was rain with a small amount of snow.

In the experiment called Graupel2, riming growth of snow must exceed depositional growth by a factor of 3 before rimed snow is transferred to the graupel category, whereas CONTROL required a unity ratio. The difference between these two threshold ratios is shown in Fig. 2c, with CONTROL represented by the 1.0 curve and Graupel2 represented approximately halfway between the 0.2 and 0.4 curves. Results of this test reveal no graupel but 73% more snow, 18% less cloud water, and 34% less cloud ice than CONTROL (see Table 2). The decrease in cloud ice is due to the lack of ice multiplication, a direct consequence of eliminating graupel since riming growth does not attain the new threshold requirement. Similar to Graupel1, snow mass increases due to deposition at the expense of cloud water.

g. Version2 experiment

As discussed in section 2, a significant number of modifications have been made to the MM5 microphysics scheme since RRB. In an experiment referred to as Version2, the code is modified to approximate RRB; however, an exact match is not possible because of bug fixes. In its simplest form, the modifications to CONTROL combine three of the sensitivity experiments above: Fletcher, Kessler5, and Graupel1. Not surprisingly, the resulting hydrometeor amounts (Table 2) are very similar to the Graupel1 experiment since little sensitivity was noted between CONTROL and Fletcher or Kessler5.

h. Snow intercept parameter: SON and SONV experiments

In sensitivity experiment SON, $N_{o,s}$ is set constant to its maximum value, 2.0×10^7 m^{-4}. This simulation produces only 9% more snow but no other discernible differences in resulting hydrometeor mixing ratios versus CONTROL. This is logical because the relatively small mixing ratio of snow produced by this shallow cloud is insufficient to reduce $N_{o,s}$ in CONTROL (es-

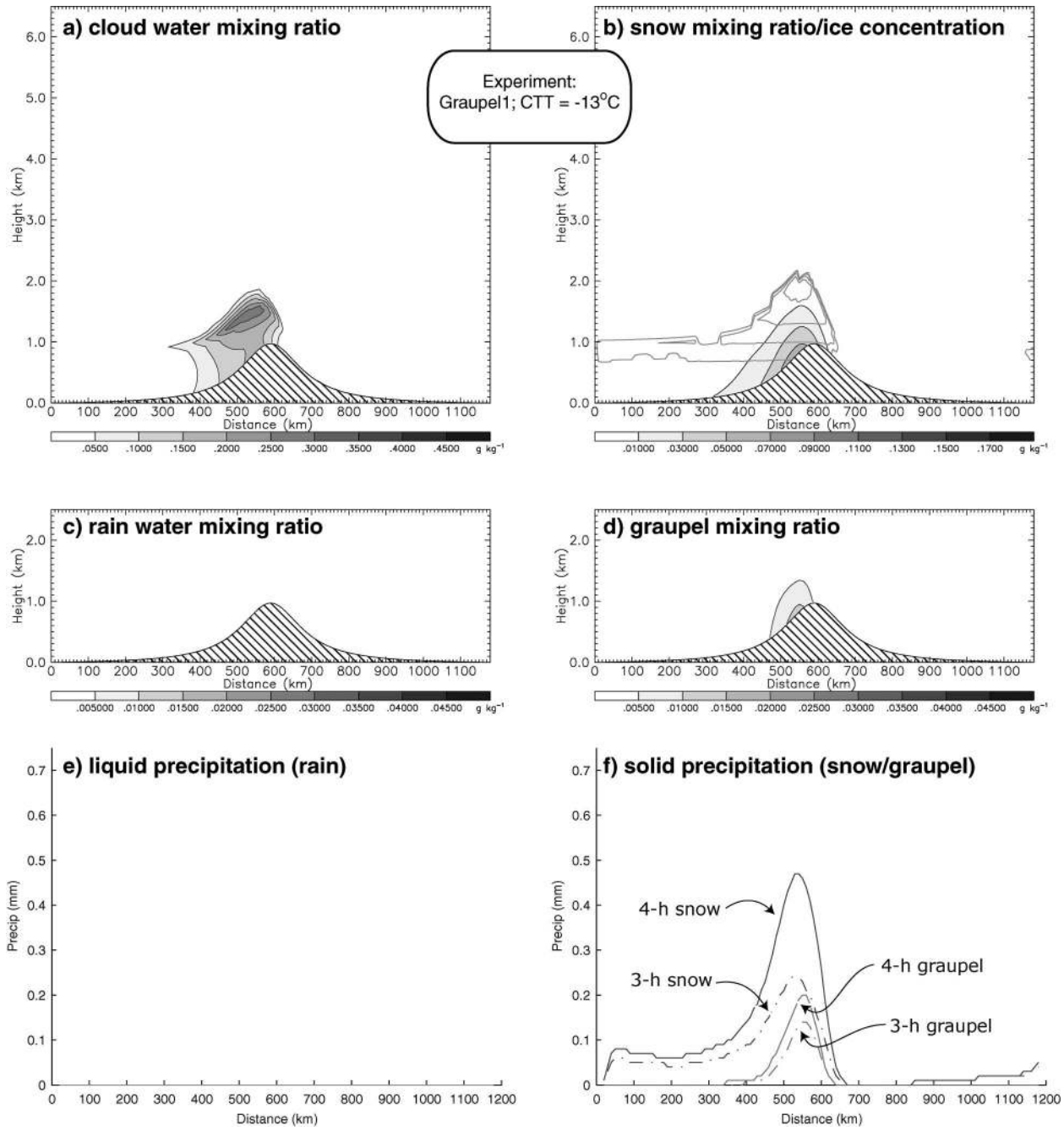

FIG. 9. Vertical cross sections from experiment Graupel1 at 3 h using CTT = −13°C sounding (Fig. 5a); otherwise same as Fig. 6.

sentially $N_{o,s}$ is constant in CONTROL); however, the impacts of this sensitivity test are apparent in the deeper and colder cloud systems discussed later.

In experiment SONV, $N_{o,s}$ depends on temperature via Eq. (13) replacing the RRB mass-dependent relationship, resulting in significant differences versus CONTROL. The maximum cloud water mixing ratio realized in this test is 0.397 g kg^{-1}, with an order of magnitude less snow, 22% less graupel, and dramatically increased rain (nearly half of the precipitation is freezing drizzle) compared to CONTROL. This result (shown in Fig. 10) compares favorably to the RG study except for the larger amounts of graupel in this simulation. The dramatic decrease in snow mixing ratio is due to a reduced depositional growth of snow (recall Fig. 3a) because the snow size distribution is shifted toward large sizes at relatively high temperatures (and the slope of the distribution decreases).

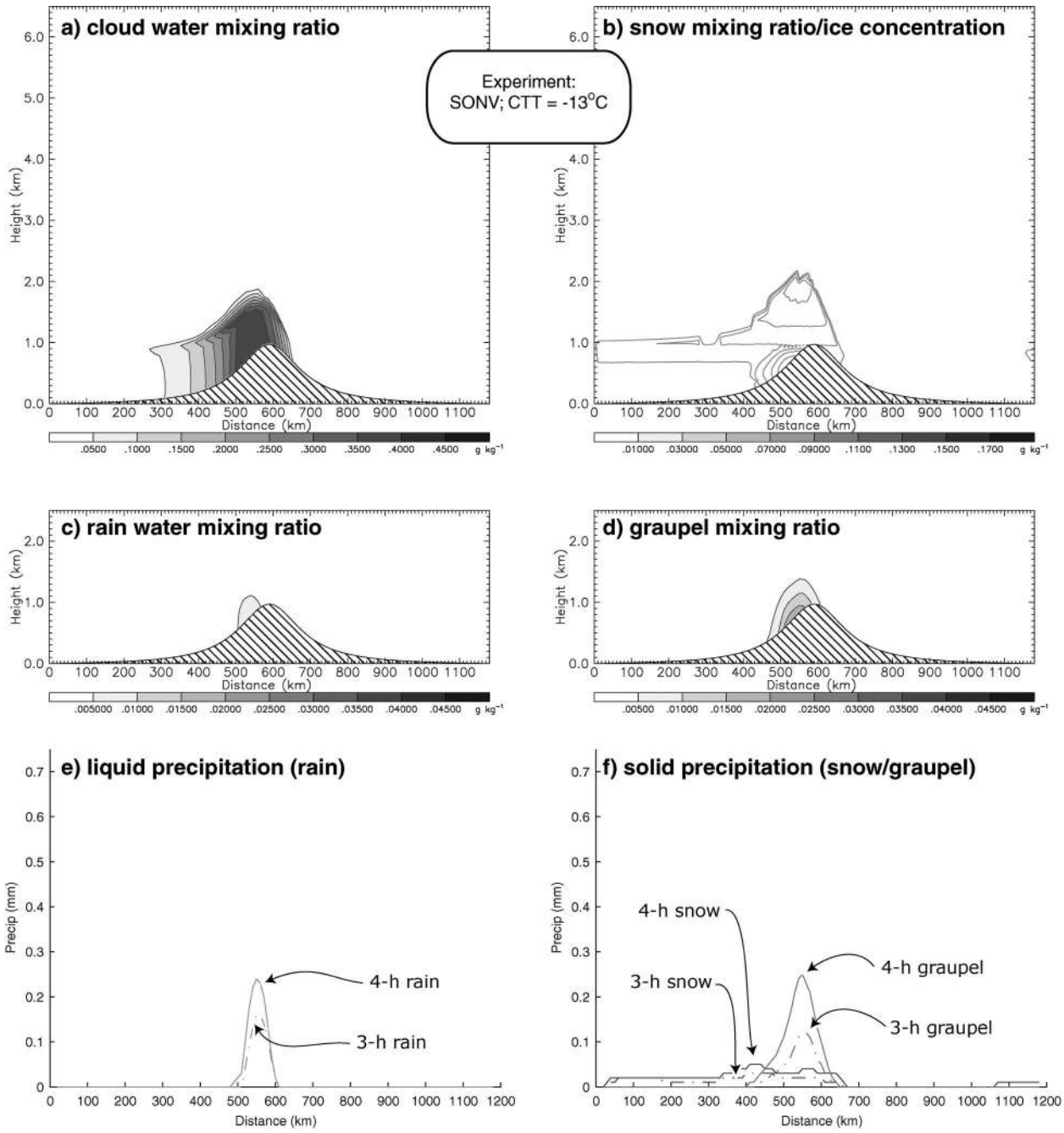

FIG. 10. Vertical cross sections from experiment SONV at 3 h using CTT = −13°C sounding (Fig. 5a); otherwise same as Fig. 6.

i. Rain intercept parameter: RON and RONV experiments

Similar to the previous modifications to the intercept parameter of snow, the intercept parameter of rain, $N_{o,s}$ is altered from 8.0×10^6 m^{-4} in CONTROL to 1.0×10^{10} m^{-4} in the sensitivity experiment referred to as RON. Testing this parameter without significant rain is meaningless, so this experiment also combines the modifications of SONV, whose simulation produces the most rainwater. From the discussion in section 2e and Fig. 4, note that the impact of this change to $N_{o,r}$ alters the terminal velocity of rain from approximately 2 to 0.5 m s^{-1} (for the amount of rain produced in SONV). The resulting cloud water at 3 h shown in Fig. 11a is 4% less than the cloud water produced in SONV (Fig. 10) because rain falls more slowly in RON, thus accreting more cloud water. Accordingly, the resulting rain accumulation is ~50% greater in RON (Fig. 11e), and the amount of rain suspended within the cloud is an order

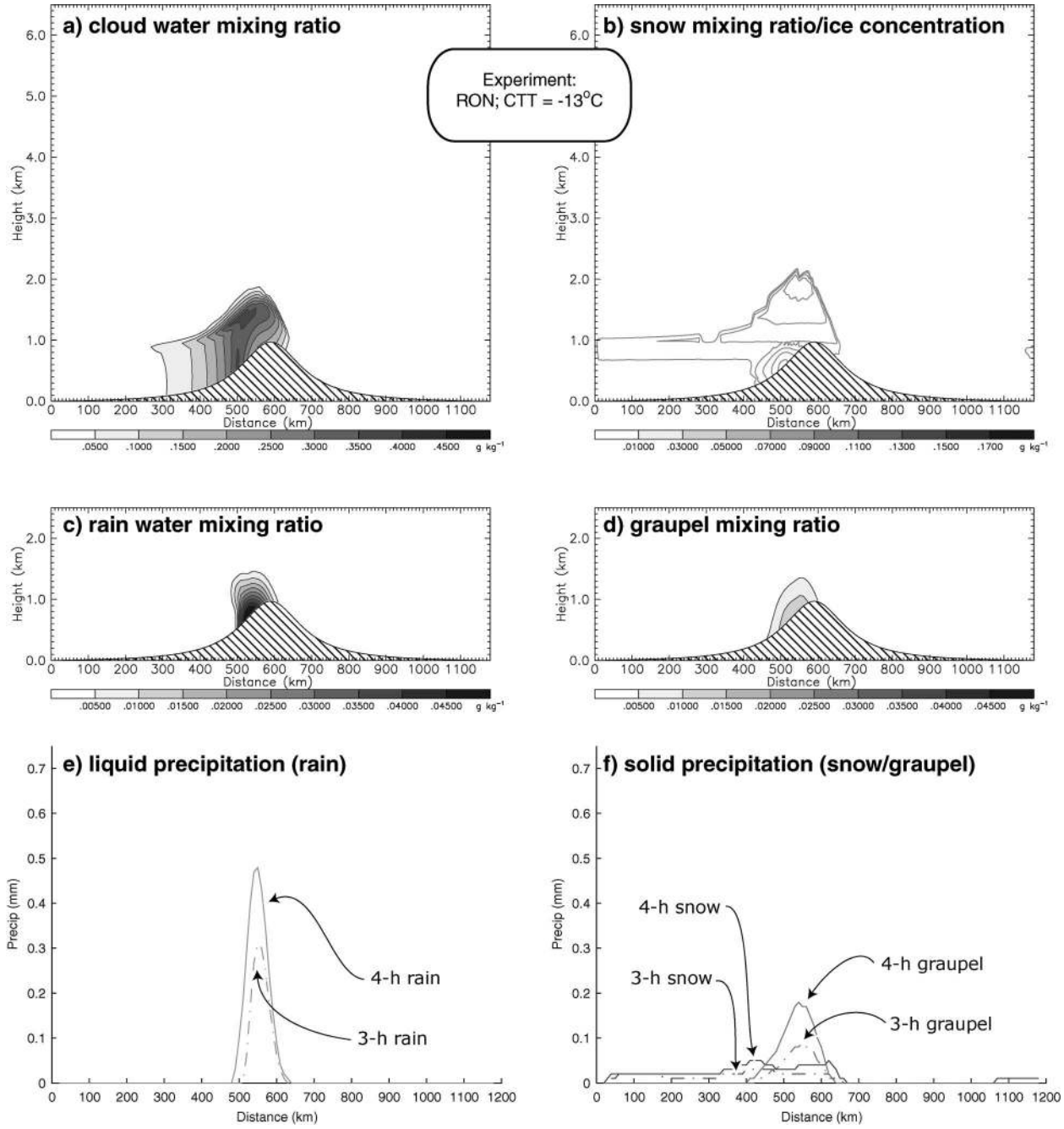

FIG. 11. Vertical cross sections from experiment RON at 3 h using CTT = −13°C sounding (Fig. 5a); otherwise same as Fig. 6.

of magnitude larger (~0.07 g kg^{-1}; Fig. 11c). The suspended rain mixing ratio is significantly increased in this simulation as compared to SONV because of the lower terminal velocity of raindrops.

In the experiment referred to as RONV, $N_{o,r}$ varies between the values used in experiments RON and CONTROL according to Eq. (14). As shown in Table 2, the resulting mixing ratios are essentially identical compared to RON because the rain mixing ratio does not increase sufficiently to impact (decrease) $N_{o,r}$.

To see the ramifications of a variable intercept parameter, we repeated the RONV experiment without any ice microphysics active, thus allowing higher cloud water and rain mixing ratios to develop. Furthermore, we aim to reproduce results by RG in association with CCN spectra sensitivities duplicated here in Fig. 12a. Note that while using a maritime CCN spectrum, their cloud water increased to ~0.4 g kg^{-1} before the onset of rain (drizzle) at approximately 1 h. When RG switched to a continental CCN spectrum, their cloud water rose to

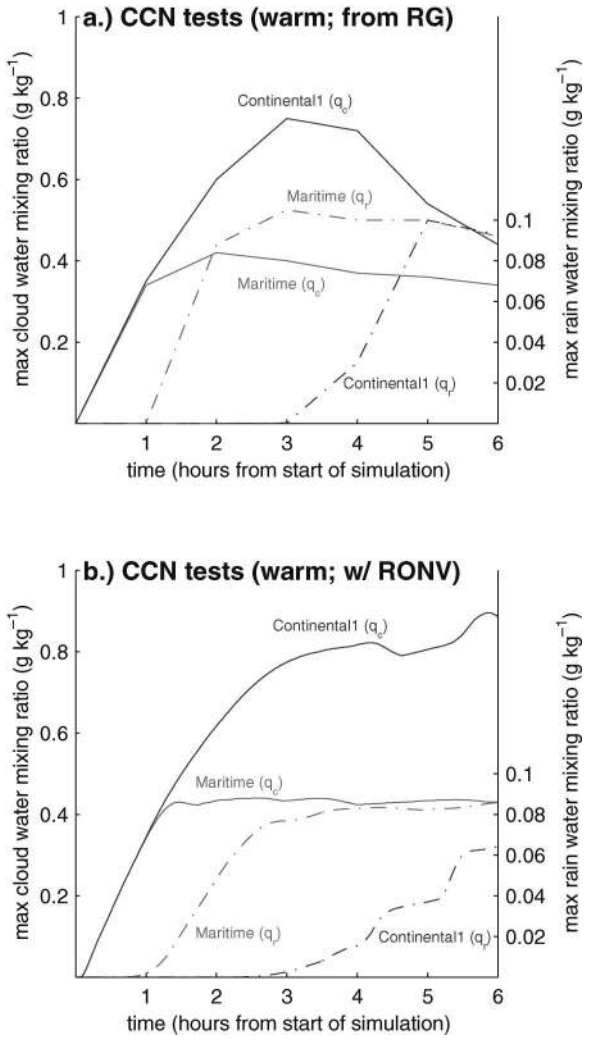

FIG. 12. Time series of cloud water (q_c—left abscissa; solid lines) and rain (q_r—right abscissa; dashed lines) mixing ratios (g kg^{-1}) using maritime and continental CCN spectra: (a) identical to Fig. 6 of Rasmussen et al. (2002) provided for comparison and (b) results when $N_{o,r}$ depends on rain mixing ratio as in experiment RONV.

$\sim$0.7 g kg^{-1} and required 3 h before producing rain. In either case, the rain mixing ratio rapidly increased to approximately 0.1 g kg^{-1} then remained nearly constant. When the RG sounding is used in an all-warm version of the bulk model using the code in experiment BandR (recall section 4d), the resulting cloud water mixing ratios are in reasonable agreement with results by RG, but the rain mixing ratios are a factor of 10 too low (cf. Fig. 8b to Fig. 12a). This is due to the large terminal velocity of rain ($\sim$3 m s^{-1}) when the intercept parameter is set constant at its classical value (8×10^6 m^{-4}); hence, rain is rapidly precipitating to the ground and not remaining suspended aloft like drizzle, as it is in the RG study. When the intercept parameter is altered to depend on mixing ratio, an experiment combining the all-warm BandR and RONV codes produces results in closer agreement to RG as shown in Fig. 12b.

j. Final experiment

Finally, in the last sensitivity simulation, the code modifications of BandR (with $N_c = 100$ cm^{-3}), Graupel2, SONV, and RONV combine to produce the experiment called Final. Results of this test (see Fig. 13 and Table 2) show a slight increase in cloud water (5%), a sharp decrease in rainwater (73%), significantly more snow (nearly an order of magnitude), and less graupel (14%) compared to RONV. Changes to the liquid portion are primarily due to swapping the autoconversion scheme, while the balance between snow and graupel is primarily due to the higher threshold for producing graupel in the Graupel2 portion of the code.

More important than comparing Final to RONV is the comparison of the Final experiment to the bin model (recall Fig. 7). While individual mixing ratios of each microphysical species do not perfectly agree, the balance of liquid and frozen species matches more closely than any other experiment. This is confirmed by the rmse values found in Table 2 as well as visual inspection of Figs. 7a–f and 13a–f.

k. Deeper/colder cloud systems

Besides testing a shallow cloud with cloud-top temperature of -13°C, tests are performed with deeper and colder cloud systems. In the remainder of this section, the temperature profile remains the same as before, but the moisture profile is altered to produce cloud systems of various depths and temperatures. Furthermore, a subset of the sensitivity studies (see Table 1) are repeated to reveal responses due to both cloud depth/temperature as well as the treatment of certain aspects of the microphysical parameterization. There is little reason to perform the full suite of tests because a few of the previous tests require sufficient cloud water or rain to exist, which, as will soon be shown, is lacking in these deeper/colder clouds.

1) CTT = -25°C

The first test moistens the profile to ice saturation from the barrier height to the altitude of the -20°C level (recall Fig. 5b). The resulting cloud (reaching $T = -25$°C) is primarily composed of ice and snow with very low cloud water mixing ratio (Fig. 14 and Table 3). Except for a brief time early in the cloud evolution, the reduced cloud water does not rime snow sufficiently to convert into graupel, and the principal precipitation type at the ground is snow.

Tests were conducted using the Meyers and Fletcher sensitivity simulations, but the results (not shown) were negligibly different from CONTROL except for the expected differences in number concentration of ice due to the temperature within the cloud. The resulting snow was no different than CONTROL because there were roughly equivalent ice number concentrations at cloud top using all three schemes (recall Fig. 1).

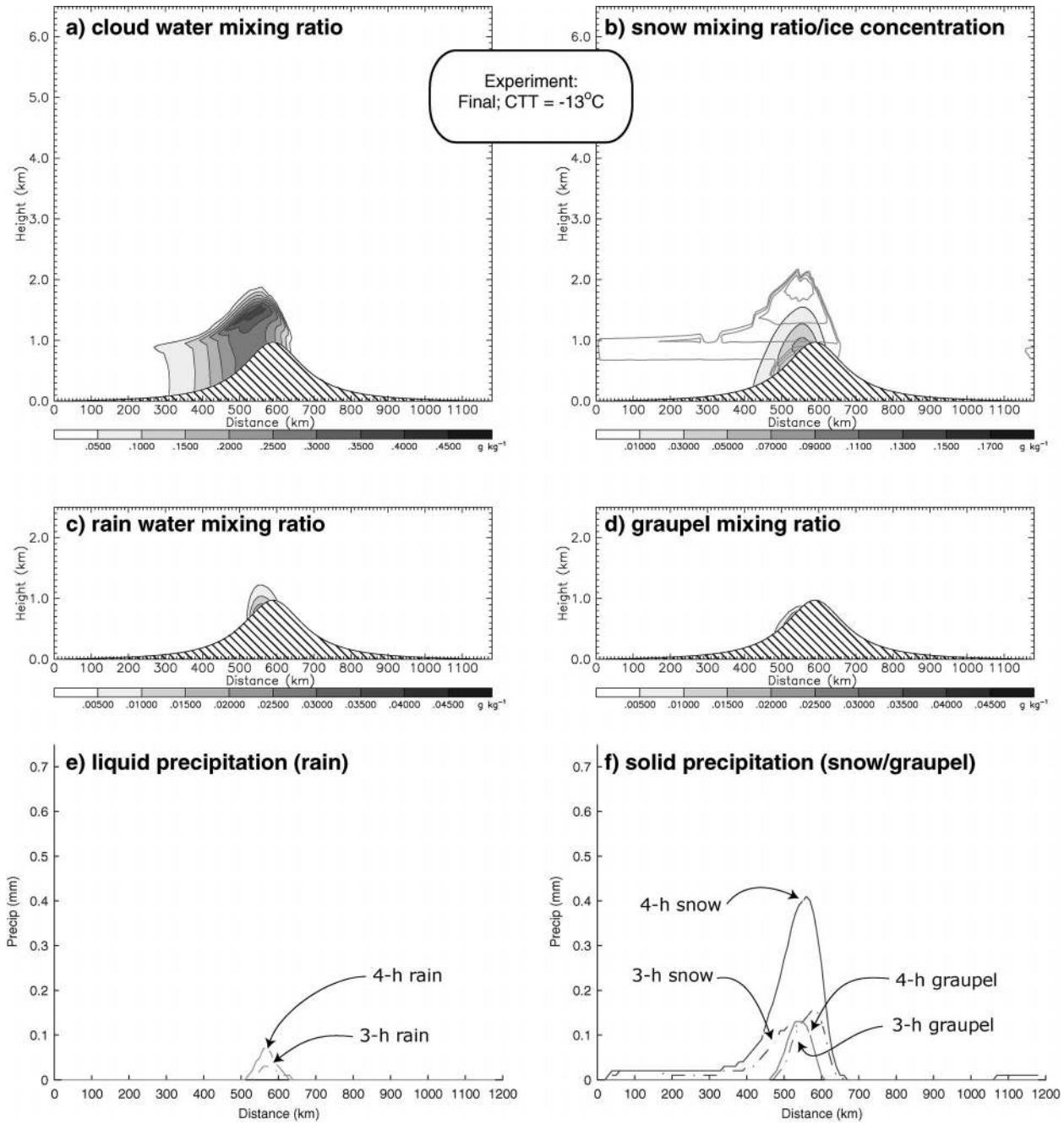

FIG. 13. Vertical cross sections from experiment Final at 3 h using CTT = −13°C sounding (Fig. 5a); otherwise same as Fig. 6.

Repeating the Graupel1 test using the original, exponential size distribution along with the original conversion of rimed snow to graupel produces 9% less cloud water, 5% less snow, and much more graupel compared to CONTROL (see Table 3). The Graupel2 test with more restrictive rimed snow to graupel conversion eliminates the very small quantity of graupel previously found in CONTROL.

When the Fletcher, Kessler5, and Graupel1 experiments are combined to create the Version2 test, the results replicate the sensitivity found in the warmer cloud—namely, results of Version2 are negligibly different from Graupel1.

Repeating the SON test results in a third as much cloud water and 28% more snow versus CONTROL plus 15% more snow accumulation. This is expected since $N_{o,s} = 2 \times 10^7$ m^{-4} causes snow to grow quicker than the RRB mass-dependent relationship that decreases $N_{o,s}$ as the snow mass increases in the deeper cloud system.

Finally, in SONV with its temperature-dependent $N_{o,s}$,

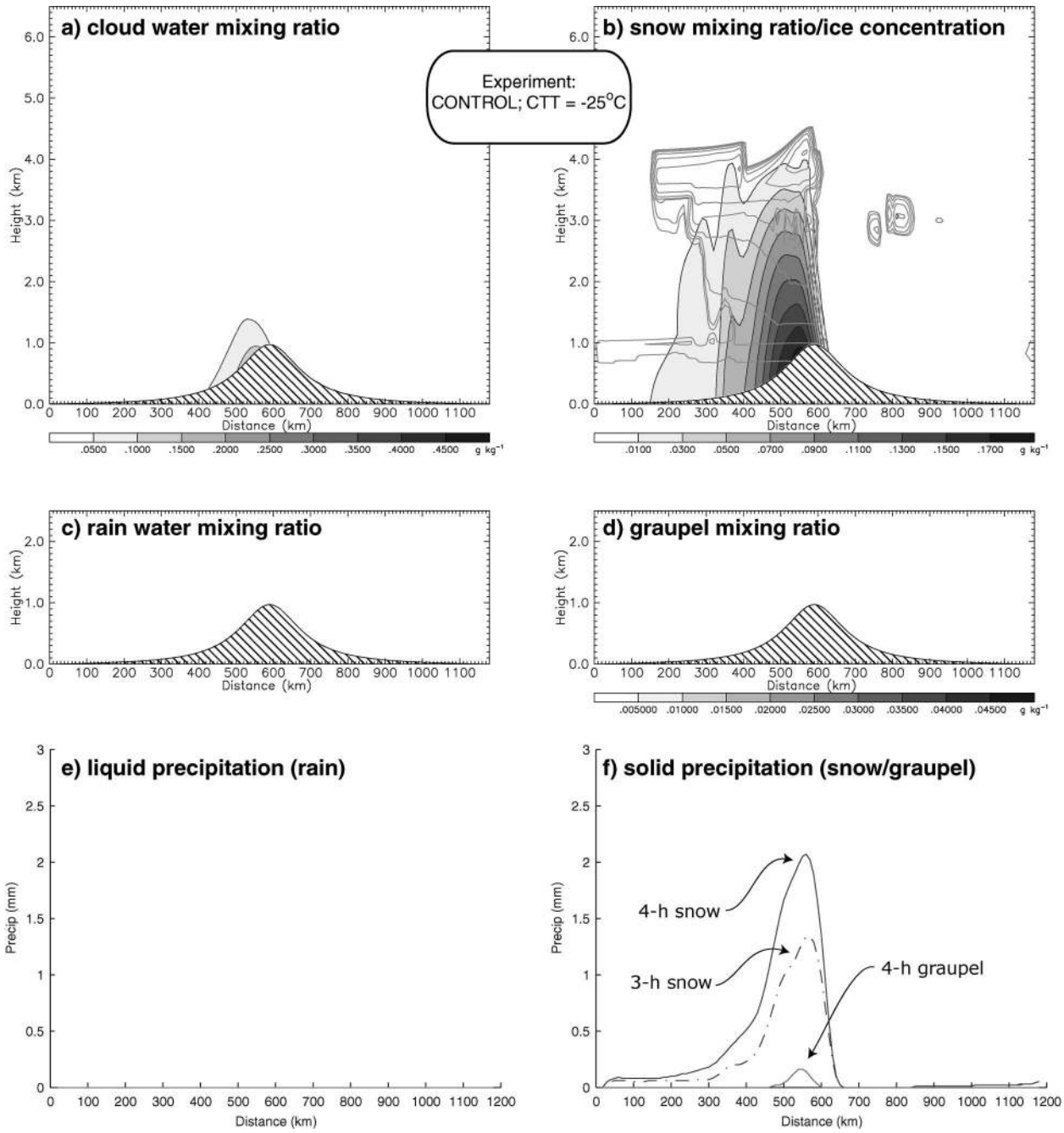

FIG. 14. Vertical cross sections from experiment CONTROL at 3 h using CTT = −25°C sounding (Fig. 5b); otherwise same as Fig. 6, except the scale of the abscissa is increased.

results show a 17% increase in cloud water and 22% increase in snow over CONTROL, with a slightly more narrow precipitation imprint on the barrier (Fig. 15 and Table 3). The higher amounts of cloud water and snow result in a trace amount of graupel. While the maximum cloud water mixing ratio (0.324 g kg^{-1}) nearly attains that of the CONTROL simulation for the shallow cloud, this water cloud rapidly glaciates to produce a realistic time evolution of the cloud. Not surprisingly, combining the SONV test with Graupel2, RONV, and BandR to re-create the Final experiment nearly eliminates all graupel.

2) CTT = −60°C

Increasing the depth of the cloud to either the −40° or −60°C level produces two orders of magnitude more

TABLE 3. As in Table 2, domain-maximum hydrometeor quantities from 2D sensitivity simulations of various cloud depths and temperatures.

Cloud system	q_c (g kg^{-1})	q_i ($\times 10^{-3}$ g kg^{-1})	N_i (L^{-1})	q_r (g kg^{-1})	q_s (g kg^{-1})	q_g (g kg^{-1})
CONTROL						
CTT = −25°C	0.114 (0.240)	0.64 (3.5)	5.8 (40)	0.000 (0.000)	0.177 (0.182)	0.000 (0.029)
CTT = −60°C	0.109 (0.240)	34 (49)	1120 (1190)	0.000 (0.000)	0.205 (0.215)	0.000 (0.028)
Seeder–feeder	0.308 (0.383)	35 (46)	1110 (1190)	0.000 (0.004)	0.160 (0.186)	0.040 (0.049)
Fletcher						
CTT = −60°C	0.109 (0.241)	15 (16)	124 (145)	0.000 (0.000)	0.207 (0.219)	0.000 (0.028)
Meyers						
CTT = −60°C	0.110 (0.226)	2.6 (10)	26 (104)	0.000 (0.000)	0.199 (0.206)	0.000 (0.026)
Graupel1						
CTT = −25°C	0.104 (0.226)	0.63 (3.5)	5.8 (40)	0.000 (0.000)	0.168 (0.173)	0.011 (0.012)
CTT = −60°C	0.100 (0.226)	34 (49)	1110 (1190)	0.000 (0.000)	0.195 (0.204)	0.012 (0.014)
Seeder–feeder	0.314 (0.383)	35 (46)	1130 (1190)	0.000 (0.004)	0.173 (0.182)	0.012 (0.021)
Graupel2						
CTT = −25°C	0.114 (0.225)	0.64 (3.5)	5.5 (40)	0.000 (0.000)	0.177 (0.181)	0.000 (0.000)
CTT = −60°C	0.109 (0.225)	34 (49)	1120 (1190)	0.000 (0.000)	0.205 (0.215)	0.000 (0.000)
Seeder–feeder	0.276 (0.370)	35 (46)	1130 (1190)	0.000 (0.017)	0.174 (0.185)	0.000 (0.002)
Version2						
CTT = −25°C	0.102 (0.225)	1.4 (13)	13 (123)	0.000 (0.000)	0.167 (0.173)	0.011 (0.012)
SON						
CTT = −25°C	0.031 (0.240)	0.64 (3.5)	6.2 (41)	0.000 (0.000)	0.227 (0.265)	0.000 (0.031)
CTT = −60°C	0.028 (0.240)	34 (39)	1140 (1190)	0.000 (0.000)	0.269 (0.296)	0.000 (0.030)
Seeder–feeder	0.306 (0.383)	35 (46)	1130 (1190)	0.000 (0.004)	0.264 (0.265)	0.043 (0.055)
SONV						
CTT = −25°C	0.133 (0.324)	0.57 (3.4)	5.5 (39)	0.000 (0.000)	0.216 (0.222)	0.009 (0.040)
CTT = −60°C	0.119 (0.328)	33 (47)	1150 (1200)	0.000 (0.000)	0.258 (0.293)	0.006 (0.041)
Seeder–feeder	0.336 (0.400)	34 (44)	1110 (1190)	0.001 (0.008)	0.186 (0.219)	0.056 (0.058)
Final						
CTT = −25°C	0.125 (0.288)	0.57 (3.4)	5.5 (39)	0.000 (0.000)	0.215 (0.221)	0.000 (0.000)
CTT = −60°C	0.113 (0.288)	33 (47)	1110 (1190)	0.000 (0.000)	0.257 (0.291)	0.000 (0.011)
Seeder–feeder	0.328 (0.429)	34 (44)	1110 (1190)	0.004 (0.006)	0.207 (0.213)	0.014 (0.044)

cloud ice (mass and number concentration), a very small decrease in cloud water (~4%), and somewhat larger increase in snow mixing ratio (~16%) and snow precipitation for all the tests in a nearly uniform manner (Table 3). An exception is the SON sensitivity experiment that produces about 11% less cloud water when the cloud increases depth from the −25°C to the −60°C level. Results of the SONV experiment (shown in Fig. 16 and Table 3) also reveal an 11% decrease in cloud water mixing ratio between the two cloud depths, but SONV maintains a low liquid-water cloud whereas SON nearly eliminates all traces of cloud water. The Final experiment produces the same sensitivity found in the −25°C cloud simulation and nearly eliminates the small amount of graupel.

3) SEEDER–FEEDER CLOUD SYSTEM

Using the same sounding as the CTT = −60°C test and altering the moisture between 1 and 3 km by decreasing the dewpoint temperature 3°C below ice saturation produces a classic seeder–feeder-type cloud system. Between 0 and 2 h, the two clouds remain distinct, with an entirely ice and snow cloud at high levels and a mixed-phase cloud similar to the original, relatively warm, and mostly water cloud adjacent to the barrier. As time progresses though, the snow formed in the upper cloud falls and reaches the lower cloud, causing the mostly water cloud to glaciate.

The individual sensitivity experiments nearly duplicate the sensitivities shown in the last section, but the amount of cloud water in the shallow, low-level cloud adjacent to the barrier is greater than the CTT = −60°C test, as this cloud initially grows independent of the upper ice/snow cloud. However, because the upper cloud does begin to interact with the lower cloud after 2 h, the cloud water is depleted more rapidly in the seeder–feeder cloud than in the original CTT = −13°C cloud. As expected, the seeder–feeder simulation looks nearly identical to the CTT = −60°C simulation beyond 4 h. SONV and Final attain the highest cloud water mixing ratio of all experiments, consistent with the other cloud depths and temperatures. In fact, the Final simulation produces a minute amount of freezing drizzle just prior to glaciation by the upper cloud (Fig. 17).

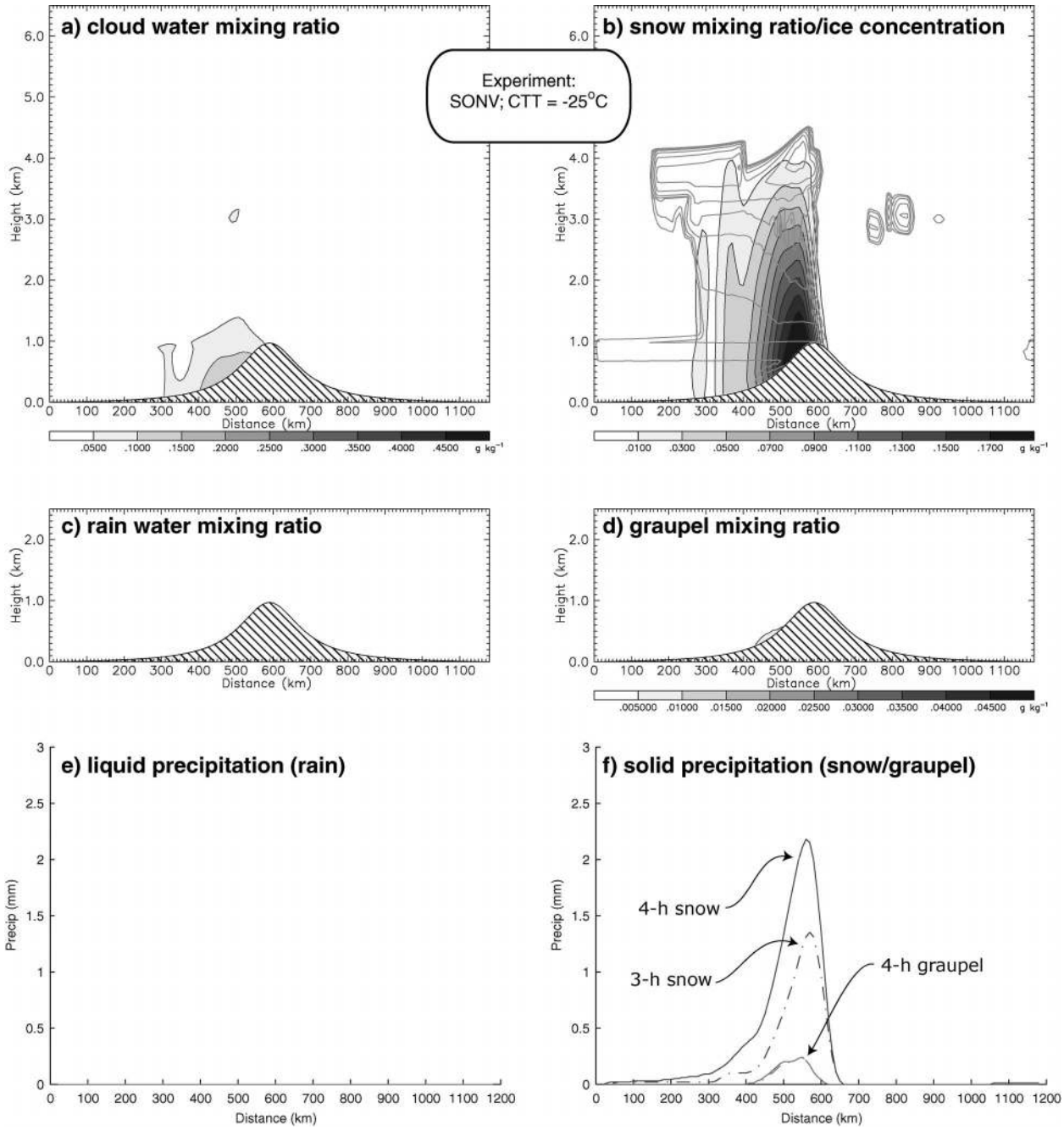

FIG. 15. Vertical cross sections from experiment SONV at 3 h using CTT = −25°C sounding (Fig. 5b); otherwise same as Fig. 14.

5. Conclusions

In summary, the bulk, mixed-phase microphysical parameterization described in Reisner et al. (1998) was rigorously tested using sensitivity experiments with idealized flow over a two-dimensional barrier. Improvements to the bulk scheme were made in order to reproduce results of the bin microphysics model of Rasmussen et al. (2002). Key improvements are the following:

- primary ice nucleation using Eq. (2), as in Cooper (1986), replaces the Fletcher (1962) curve;
- autoconversion using Eq. (6), as in Walko et al. (1995), replaces the Kessler (1969) scheme;
- a generalized gamma distribution for graupel using Eq. (8) replaces the exponential distribution; the associated intercept parameter depends on mixing ratio using Eq. (10) instead of remaining constant; and riming growth of snow must exceed depositional growth

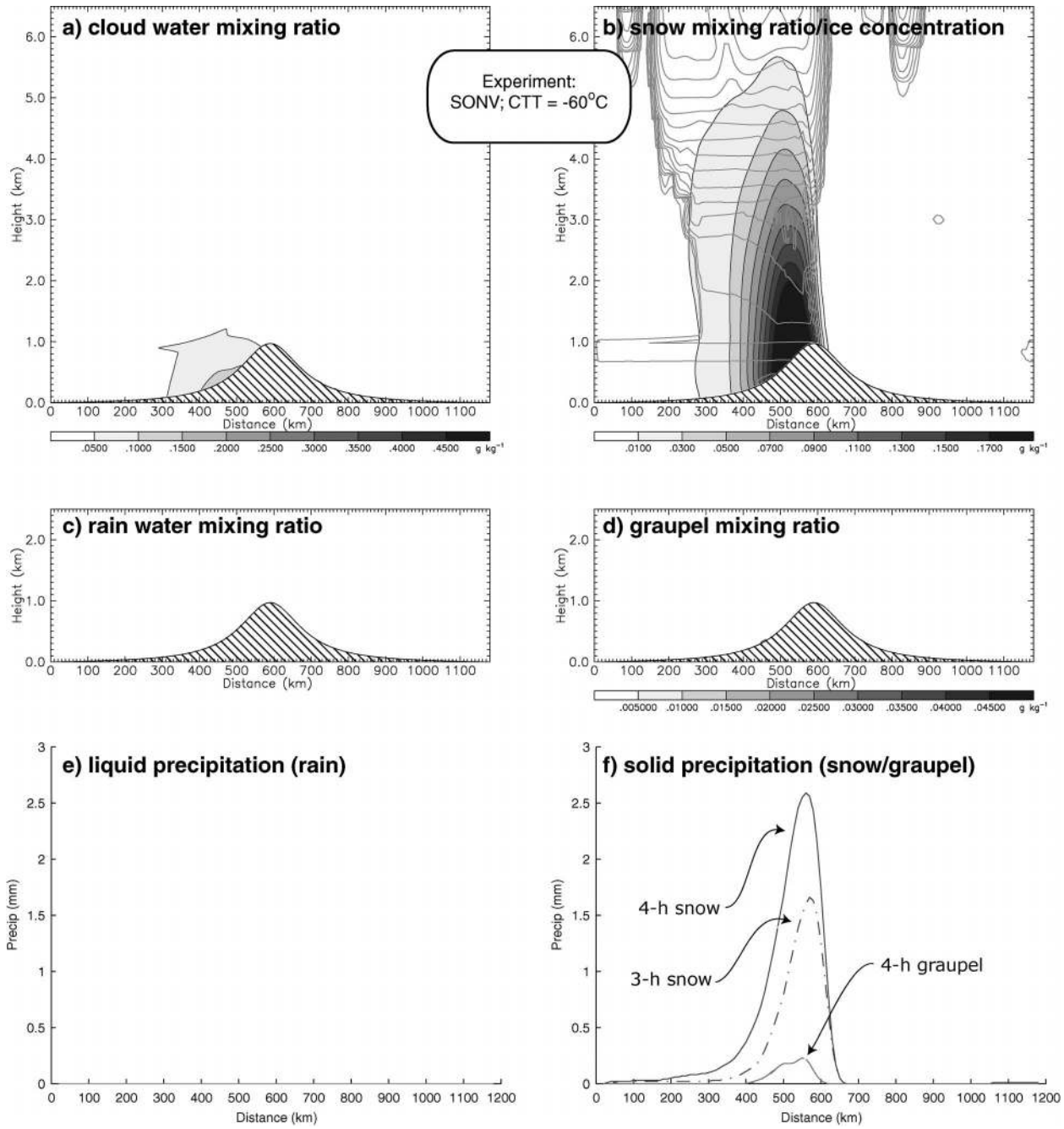

FIG. 16. Vertical cross sections from experiment SONV at 3 h using CTT = −60°C sounding (Fig. 5c); otherwise same as Fig. 14.

of snow by a factor of 3 before rimed snow transfers into the graupel category;
- the intercept parameter of the snow size distribution depends on temperature using Eq. (13) replacing the mixing ratio dependency;
- the intercept parameter for the rain size distribution depends on rain mixing ratio, thereby simulating the fall velocity of drizzle drops as well as raindrops.

Tests of three ice initiation schemes producing an order of magnitude different numbers of ice crystals revealed little sensitivity when simulating deep and cold cloud systems having cloud-top temperatures less than −25°C but more sensitivity when simulating relatively warm cloud systems (the most sensitivity was seen at temperatures between 0° and −10°C). In particular, the Meyers et al. (1992) scheme, which produced the most

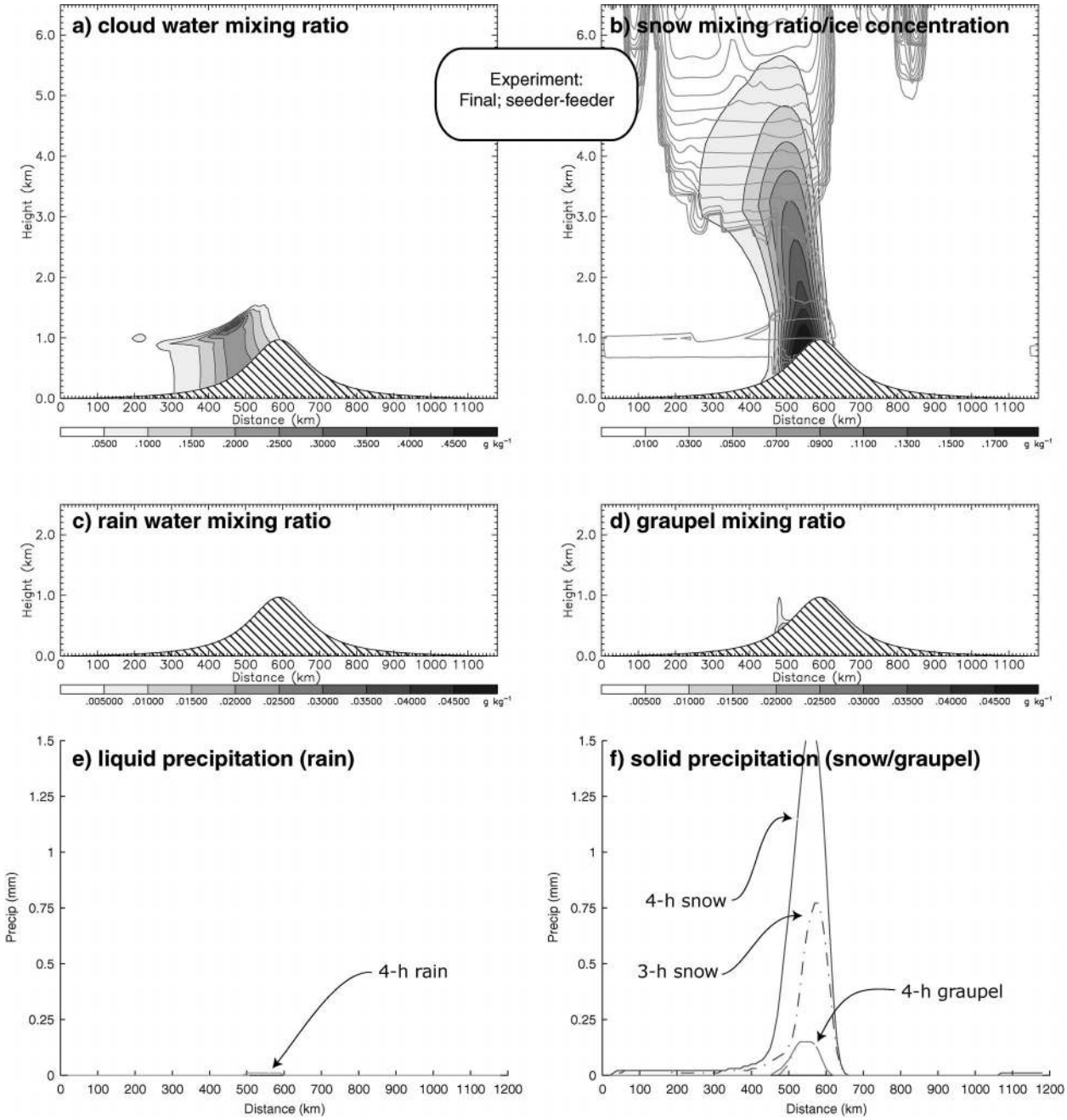

FIG. 17. Vertical cross sections from experiment Final at 3 h using seeder–feeder sounding (Fig. 5d); otherwise same as Fig. 13, except the scale of the abscissa is increased.

ice crystals, depleted the most cloud water as expected. For this reason and since Cooper (1986) directly measured ice crystal concentrations, we chose to use the Cooper curve to initiate ice by deposition nucleation for the final microphysics code.

A series of tests using simplistic, commonly used autoconversion methods to convert cloud water to the rain category showed the anticipated result of increasing (decreasing) cloud water (drizzle) content with increasing cloud droplet concentration (a proxy variable for CCN). One exception was the Kessler (1969) scheme since it converts cloud water to rain based on attaining a threshold cloud water content and contains no dependence on droplet concentration. In the end, we chose to use the Walko et al. (1995) adaptation of a Berry and Reinhardt (1974) autoconversion scheme since it represents the fundamental process of drizzle formation as a function of CCN. In cases where the CCN spectrum

is known, we advise modelers to set an appropriate value for N_c, otherwise we advise setting $N_c = 100$ cm^{-3} for general use as a compromise between maritime and continental CCN spectra. In the future, we intend to preset the value of N_c based on surface characteristics (proximity to land/sea/ice/urban regions) and/or boundary layer depth and advect this quantity to allow for inhomogeneous CCN spectra. Also in the future, we plan to test a scheme proposed by Khairoutdinov and Kogan (2000) with more sophisticated treatment for converting cloud water to rain.

In the next series of sensitivity experiments, two aspects pertaining to the treatment of graupel were tested, and the balance of cloud water, snow, and graupel was found to be very sensitive. First, the assumed size distribution was altered from an exponential distribution to a generalized gamma distribution. When an exponential distribution was used, the simulations produced more graupel and did not compare as favorably to results by the bin model as when a gamma distribution was used, primarily due to depositional growth by small graupel particles. Second, the conversion of rimed snow to graupel was altered to eliminate a dependence on model time step. The final code now consists of a combination of ideas by Murakami (1990) and Rutledge and Hobbs (1984) whereby rimed snow does not convert to graupel until the riming growth rate is 3 times larger than the depositional growth rate of snow. This requirement produced results in closer agreement to the bin model, but it still lacks a solid physical basis. In the future, we anticipate analyzing aircraft data from the Improvement of Microphysical Parameterizations through Observational Verification Experiments (IMPROVE) field projects (Stoelinga et al. 2004) to attempt a more physical consideration of graupel initiation from rimed snow.

Of the numerous sensitivity experiments, the series testing the intercept parameter of the snow size distribution caused the largest change in cloud water and resulting formation of freezing drizzle. When the intercept parameter was altered from a dependence on mass to a dependence on temperature following observed data by Houze et al. (1979), the maximum cloud water mixing ratio increased from 0.18 to 0.39 g kg^{-1} (using the original RG sounding, while much less sensitivity was found in the CTT $= -13$°C sounding). The increase led to the formation of rain, essentially freezing drizzle, that correlated well with the results of the bin model. However, since the rain intercept parameter was set rather low for the extremely low rain precipitation rate, the rain resulting from experiment SONV quickly fell to the ground. Therefore, a final modification was to make the rain distribution's intercept parameter a function of the rain mixing ratio in order to simulate the lower terminal velocities associated with drizzle. This type of treatment is lacking in nearly all bulk microphysical parameterizations. The results from this simulation gave the best agreement with the bin model and is the recommended configuration of the scheme.

Besides the set of 3D simulations of various winter storm systems reported in the forthcoming companion paper, we intend to simulate a number of the cases from the IMPROVE-1/2 observation campaigns. The IMPROVE project collected an immense amount of in situ and remote measurements of cloud microphysical data for the primary purpose of improving numerical models' bulk representation of microphysics.

Acknowledgments. The authors wish to thank Bill Hall, Istvan Geresdi, John Brown, Stewart Cober, Matt Garvert, Brain Colle, Mark Stoelinga, Guenther Zaengl, Marcia Politovich, and Gerhard Kramm for their valuable contributions to this work. This research is in response to requirements and funding by the Federal Aviation Administration. The views expressed are those of the authors and do not necessarily represent the official policy or position of the FAA.

APPENDIX

Corrections and Additions to Reisner et al. (1998)

Besides the major changes discussed in section 2, the following list contains corrections and minor additions to Reisner et al. (1998):

- Eq. (A.7): The term P_{icns} should be positive, not negative.
- Eq. (A.29): N_i should be divided by ρ (in numerator).
- Eq. (A.36): A' should state $L_s^2\ \rho$ (in numerator).
- Eqs. (A.36) and (A.62): $S_c^{1/3}$ is missing (also missing in Rutledge and Hobbs 1983); appears correctly here in Eq. (11).
- Eq. (A.42): $\underline{\rho_i}$ should be ρ_w (in numerator).
- Eq. (A.48): $\overline{U_r U_s}$ should be $\overline{U}_r \overline{U}_s$.
- Eq. (A.58): L_f should be multiplied by ρ (in denominator).
- Eq. (A.61): ρ should be omitted.
- Appendix B: μ, dynamic viscosity of air, should have units of kg m^{-1} s^{-1}.
- Eq. (A.6): Production of graupel by graupel accreting rain, P_{gacr}, using Eq. (A.13) of Rutledge and Hobbs (1983) is added.
- Appendix B and Eq. (A.29): $m_{\text{so}} = 4.4 \times 10^{-11}$ kg conflicts with a minimum radius for snow of 75 μm stated below Eq. (A.29). Using 75-μm minimum radius of snow produces $m_{\text{so}} = 1.77 \times 10^{-10}$ kg.
- Eqs. (A.36) and (A.57): Latent heat effects reduce the amount of depositional growth of snow or graupel. Previously the effect was ignored, but now it has been included following Cotton and Anthes [1989, Eqs. (4)–(37)].
- Eq. (A.19): Formulas for computing saturation mixing ratios of water and ice are replaced using the polynomial estimates of Flatau et al. (1992).
- Eqs. (A.43), (A.46), (A.59), and (A.61): In place of

constant efficiencies (1.0), efficiencies for collisions between cloud water and snow, graupel, and rain utilize a Stokes number relationship.
- Previously, any rimed snow in the appropriate temperature range triggered ice multiplication. Now, following Hobbs and Rangno (1998), graupel is required instead of rimed snow.

REFERENCES

Benjamin, S. G., and Coauthors, 2004: An hourly assimilation–forecast cycle: The RUC. *Mon. Wea. Rev.,* **132,** 495–518.

Berry, E. X., 1968: Modification of the warm rain process. *Proc. First Conf. on Weather Modification,* Albany, NY, Amer. Meteor. Soc., 81–88.

——, and R. L. Reinhardt, 1974: An analysis of cloud drop growth by collection. Part II: Single initial distributions. *J. Atmos. Sci.,* **31,** 2127–2135.

Brown, P. R., and H. A. Swann, 1997: Evaluation of key microphysical parameters in three-dimensional cloud-model simulations using aircraft and multiparameter radar data. *Quart. J. Roy. Meteor. Soc.,* **123,** 2245–2275.

Cober, S. G., G. A. Isaac, and J. W. Strapp, 2001: Characterizations of aircraft icing environments that include supercooled large drops. *J. Appl. Meteor.,* **40,** 1984–2002.

Cooper, W. A., 1986: Ice initiation in natural clouds. *Precipitation Enhancement—A Scientific Challenge, Meteor. Monogr.,* No. 43, Amer. Meteor. Soc., 29–32.

Cotton, W. R., and R. Anthes, 1989: *Storm and Cloud Dynamics.* Academic Press, 883 pp.

——, G. J. Tripoli, R. M. Rauber, and E. A. Mulvihill, 1986: Numerical simulation of the effects of varying ice crystal nucleation rates and aggregation processes on orographic snowfall. *J. Climate Appl. Meteor.,* **25,** 1658–1680.

Feingold, G. B. Stevens, W. R. Cotton, and R. L. Walko, 1994: An explicit cloud microphysics/LES model designed to simulate the Twomey effect. *Atmos. Res.,* **33,** 207–233.

——, S. Tzivion, and Z. Levin, 1998: Evolution of the raindrop spectra. Part I: Solution to the stochastic collection/breakup equation using the method of moments. *J. Atmos. Sci.,* **45,** 3387–3399.

Ferrier, B. S., 1994: A double-moment multiple-phase four-class bulk ice scheme. Part I: Description. *J. Atmos. Sci.,* **51,** 249–280.

Flatau, P. J., R. L. Walko, and W. R. Cotton, 1992: Polynomial fits to saturation vapor pressure. *J. Appl. Meteor.,* **31,** 1507–1513.

Fletcher, N. H., 1962: *The Physics of Rain Clouds.* Cambridge University Press, 386 pp.

Geresdi, I., 1998: Idealized simulation of the Colorado hailstorm case: Comparison of bulk and detailed microphysics. *Atmos. Res.,* **45,** 237–252.

Hall, W. D., 1980: A detailed microphysical model within a two-dimensional dynamical framework: Model description and preliminary results. *J. Atmos. Sci.,* **37,** 2486–2507.

Hallet, J., and S. C. Mossop, 1974: Production of secondary ice particles during the riming process. *Nature,* **249,** 26–28.

Hobbs, P. V., and A. L. Rangno, 1998: Reply to ''Comments by Alan M. Blyth and John Latham on 'Cumulus glaciation papers by P. V. Hobbs and A. L. Rangno.'" *Quart. J. Roy. Meteor. Soc.,* **124,** 1009–1011.

Houze, R. A., P. V. Hobbs, P. H. Herzegh, and D. B. Parsons, 1979: Size distributions of precipitation particles in frontal clouds. *J. Atmos. Sci.,* **36,** 156–162.

Kessler, E., III, 1969: *On the Distribution and Continuity of Water Substance in Atmospheric Circulations. Meteor. Monogr.,* No. 32, Amer. Meteor. Soc., 84 pp.

Khairoutdinov, M., and Y. Kogan, 2000: A new cloud physics parameterization in a large-eddy simulation model of marine stratocumulus. *Mon. Wea. Rev.,* **128,** 229–243.

Kogan, Y., 1991: The simulation of a convective cloud in a 3-D model with explicit microphysics. Part I: Model description and sensitivity experiments. *J. Atmos. Sci.,* **48,** 1160–1189.

Kong, F., and M. K. Yau, 1997: An explicit approach to microphysics in MC2. *Atmos.–Ocean,* **35,** 257–291.

Lin, Y. L., R. Farley, and H. D. Orville, 1983: Bulk parameterization of the snow field in a cloud model. *J. Climate Appl. Meteor.,* **22,** 1065–1092.

Meyers, M. P., and W. R. Cotton, 1992: Evaluation of the potential for wintertime quantitative precipitation forecasting over mountainous terrain with an explicit cloud model. Part I: Two-dimensional sensitivity experiments. *J. Appl. Meteor.,* **31,** 26–50.

——, P. J. DeMott, and W. R. Cotton, 1992: New primary ice-nucleation parameterizations in an explicit cloud model. *J. Appl. Meteor.,* **31,** 708–721.

——, R. L. Walko, J. Y. Harrington, and W. R. Cotton, 1997: New RAMS cloud microphysics parameterization. Part II: The two-moment scheme. *Atmos. Res.,* **45,** 3–39.

Murakami, M., 1990: Numerical modeling of dynamical and microphysical evolution of an isolated convective cloud—The 19 July 1981 CCOPE Cloud. *J. Meteor. Soc. Japan,* **68,** 107–128.

Pruppacher, H. R., and J. D. Klett, 1978: *Microphysics of Clouds and Precipitation.* D. Reidel, 714 pp.

Rasmussen, R. M., I. Geresdi, G. Thompson, K. Manning, and E. Karplus, 2002: Freezing drizzle formation in stably stratified layer clouds: The role of radiative cooling of cloud droplets, cloud condensation nuclei, and ice initiation. *J. Atmos. Sci.,* **59,** 837–860.

Reisner, J., R. M. Rasmussen, and R. T. Bruintjes, 1998: Explicit forecasting of supercooled liquid water in winter storms using the MM5 mesoscale model. *Quart. J. Roy. Meteor. Soc.,* **124,** 1071–1107.

Rutledge, S. A., and P. V. Hobbs, 1983: The mesoscale and microscale structure and organization of clouds and precipitation in midlatitude cyclones. VIII: A model for the ''seeder-feeder'' process in warm-frontal rainbands. *J. Atmos. Sci.,* **40,** 1185–1206.

——, and ——,1984: The mesoscale and microscale structure and organization of clouds and precipitation in midlatitude cyclones. XII: A diagnostic modeling study of precipitation development in narrow cold-frontal rainbands. *J. Atmos. Sci.,* **41,** 2949–2972.

Sekhon, R. S., and R. C. Srivastava, 1970: Snow spectra and radar reflectivity. *J. Atmos. Sci.,* **27,** 299–307.

Stoelinga, M. T., and Coauthors, 2004: Improvement of microphysical parameterizations through observational verification experiment. *Bull. Amer. Meteor. Soc.,* **84,** 1807–1826.

Swann, H., 1998: Sensitivity to the representation of precipitating ice in CRM simulations of deep convection. *Atmos. Res.,* **47–48,** 415–435.

Tremblay, A., A. Glazer, and L. Garand, 2001: Comparison of three cloud schemes in winter storm forecasts. *Mon. Wea. Rev.,* **129,** 2923–2938.

Verlinde, J., P. J. Flatau, and W. R. Cotton, 1990: Analytical solutions to the collection growth equation: Comparison with approximate methods and application to cloud microphysics parameterization schemes. *J. Atmos. Sci.,* **47,** 2871–2880.

Walko, R. L., W. R. Cotton, M. P. Meyers, and J. Y. Harrington, 1995: New RAMS cloud microphysics parameterization. Part I: The single-moment scheme. *Atmos. Res.,* **38,** 29–62.

Wallace, J. M., and P. V. Hobbs, 1977: *Atmospheric Science*: *An Introductory Survey.* Academic Press, 467 pp.

Young, K. C., 1974: A numerical simulation of wintertime, orographic precipitation. Part I: Description of model microphysics and numerical techniques. *J. Atmos. Sci.,* **31,** 1735–1748.

——,1993: *Microphysical Processes in Clouds.* Oxford University Press, 427 pp.